JV 31 – EVALUATION OF POTENTIAL SCR CATALYST BLINDING DURING COAL COMBUSTION AND ADD-ON: IMPACT OF SCR CATALYST ON MERCURY OXIDATION IN LIGNITE-FIRED COMBUSTION SYSTEMS

Final Report

(for the period of November 1, 2000 – June 30, 2004)

Prepared for:

AAD Document Control

U.S. Department of Energy
National Energy Technology Laboratory
PO Box 10940, MS 921-107
Pittsburgh, PA 15236-0940

Performance Monitor: Susan Maley
Cooperative Agreement No. DE-FC26-98FT40321

Submitted by:

Jason D. Laumb
Steven A. Benson
Charlene R. Crocker
Jay R. Gunderson
Robert R. Jensen

Energy & Environmental Research Center
University of North Dakota
Box 9018
Grand Forks, ND 58202-9018

04-EERC-11-09 November 2004

DOE DISCLAIMER

This report was prepared as an account of work sponsored by an agency of the United States Government. Neither the United States Government, nor any agency thereof, nor any of its employees makes any warranty, express or implied, or assumes any legal liability or responsibility for the accuracy, completeness, or usefulness of any information, apparatus, product, or process disclosed or represents that its use would not infringe privately owned rights. Reference herein to any specific commercial product, process, or service by trade name, trademark, manufacturer, or otherwise does not necessarily constitute or imply its endorsement, recommendation, or favoring by the United States Government or any agency thereof. The views and opinions of authors expressed herein do not necessarily state or reflect those of the United States Government or any agency thereof.

This report is available to the public from the National Technical Information Service, U.S. Department of Commerce, 5285 Port Royal Road, Springfield, VA 22161; phone orders accepted at (703) 487-4650.

DOE ACKNOWLEDGMENT

This report was prepared with the support of the U.S. Department of Energy (DOE) National Energy Technology Laboratory Cooperative Agreement No. DE-FC26-98FT40321. However, any opinions, findings, conclusions, or recommendations expressed herein are those of the authors(s) and do not necessarily reflect the views of DOE.

EERC DISCLAIMER

LEGAL NOTICE. This research report was prepared by the Energy & Environmental Research Center (EERC), an agency of the University of North Dakota, as an account of work sponsored by DOE. Because of the research nature of the work performed, neither the EERC nor any of its employees makes any warranty, express or implied, or assumes any legal liability or responsibility for the accuracy, completeness, or usefulness of any information, apparatus, product, or process disclosed, or represents that its use would not infringe privately owned rights. Reference herein to any specific commercial product, process, or service by trade name, trademark, manufacturer, or otherwise does not necessarily constitute or imply its endorsement or recommendation by the EERC.

NDIC DISCLAIMER

This report was prepared by the Energy & Environmental Research Center (EERC) pursuant to an agreement partially funded by the Industrial Commission of North Dakota, and neither the EERC nor any of its subcontractors nor the North Dakota Industrial Commission nor any person acting on behalf of either:

(A) Makes any warranty or representation, express or implied, with respect to the accuracy, completeness, or usefulness of the information contained in this report, or that the use of any information, apparatus, method, or process disclosed in this report may not infringe privately owned rights; or

(B) Assumes any liabilities with respect to the use of, or for damages resulting from the use of, any information, apparatus, method, or process disclosed in this report.

Reference herein to any specific commercial product, process, or service by trade name, trademark, manufacturer, or otherwise does not necessarily constitute or imply its endorsement, recommendation, or favoring by the North Dakota Industrial Commission. The views and opinions of authors expressed herein do not necessarily state or reflect those of the North Dakota Industrial Commission.

JV 31 – EVALUATION OF POTENTIAL SCR CATALYST BLINDING DURING COAL COMBUSTION AND ADD-ON: IMPACT OF SCR CATALYST ON MERCURY OXIDATION IN LIGNITE-FIRED COMBUSTION SYSTEMS

ABSTRACT

Lignite and subbituminous coals from the United States of America have characteristics that impact the performance of catalysts used in selective catalyst reduction (SCR) for nitrogen oxide removal and mercury oxidation. Typically, these coals contain ash-forming components that consist of inorganic elements (sodium, magnesium, calcium, and potassium) associated with the organic matrix and mineral grains (quartz, clays, carbonates, sulfates, and sulfides). Upon combustion, the inorganic components undergo chemical and physical transformations that produce intermediate inorganic species in the form of inorganic gases, liquids, and solids. The alkali and alkaline-earth elements are partitioned between reactions with minerals and reactions to form alkali and alkaline-earth-rich oxides during combustion. The particles resulting from the reaction with minerals produce low-melting-point phases that cause a wide range of fireside deposition problems. The alkali and alkaline-earth-rich oxides consist mainly of very small particles (<5 µm) that are carried into the backpasses of the combustion system and react with flue gas to form sulfates and, possibly, carbonates. These particles cause low-temperature deposition, blinding, and plugging problems in SCR systems. These coals also lack sufficient levels of chlorine needed to oxidize mercury. Slipstream testing was conducted at two subbituminous-fired power plants and one lignite-fired power plant to determine the impacts of ash on SCR plugging, blinding, and mercury oxidation. The results indicated a high potential for blinding and plugging because of the formation of sulfate-bonded deposits but no evidence of mercury oxidation.

TABLE OF CONTENTS

LIST OF FIGURES ii

LIST OF TABLES v

EXECUTIVE SUMMARY vi

INTRODUCTION 1

EXPERIMENTAL 2
- Thermochemical Equilibrium Modeling 2
- Bench-Scale TGA Study 3
- Slipstream Reactor Installation and Operation 3
- SEM Ash Characterization 3
- Mercury Measurement 4

RESULTS AND DISCUSSION 4
- Task 1 – Identification of Test Coals and Utility Host Sites 4
- Task 2 – Bench-Scale Testing and FACT Modeling 6
  - Bench-Scale Testing 6
  - FACT Modeling 10
  - Characterization of Reaction Products from Bench-Scale Tests 16
- Task 3 – Design and Construction of the SCR Slipstream Test Chamber 16
- Task 4 – SCR Test Chamber Installation and Data Collection at Utility Host Sites 21
  - Baldwin Station Data 23
  - Columbia Station Data 23
  - Coyote Station Data 27
  - Visual Observations and Chemical Analysis 29
  - Baldwin Station Deposits 29
  - Columbia Station Deposits 33
  - Coyote Station Deposits 35
  - Reactivity Testing 41
- Task 5 – Determination of SCR Blinding Mechanisms 41
- Add-On Task – Characterization of Mercury Transformations Across SCR Catalysts for a Lignite Coal-Fired Boiler 45
- Task 6 – Final Interpretation, Recommendations, and Reporting 49

CONCLUSIONS 51

REFERENCES 55

LIST OF FIGURES

1 Weight gain curves for Nanticoke PRB 8

2 Weight gain curves for Beulah lignite.....8

3 Weight gain curves for Nanticoke PRB–LSUS blend 9

4 Weight gain curves for Nanticoke PRB with ammonia and phosphorus compounds 11

5 Weight gain curves for Nanticoke PRB–LSUS blend with ammonia and phosphorus compounds 11

6 Weight gain curves for baseline Nanticoke PRB and Nanticoke PRB with catalyst.....12

7 Weight gain curves for baseline LSUS–Nanticoke PRB blend and LSUS–Nanticoke PRB blend with catalyst. 12

8 FACT modeling results for Nanticoke PRB with 300 ppm ammonia and 1000 ppm P_2O_5 13

9 FACT modeling results for Nanticoke PRB–LSUS blend with 300 ppm ammonia and 1000 ppm P_2O_5 13

10 FACT modeling results for Beulah with 300 ppm ammonia and 1000 ppm P_2O_5 14

11 FACT modeling results for Nanticoke PRB with 100 ppm ammonia and 1 ppm P_2O_5.....14

12 FACT modeling results for Nanticoke PRB–LSUS blend with 100 ppm ammonia and 1 ppm P_2O_5 15

13 FACT modeling results for Beulah with 100 ppm ammonia and 1 ppm P_2O_5 15

14 SEM micrograph of reaction products from Nanticoke PRB 17

15 SEM micrograph of reaction products from Nanticoke PRB–LSUS blend.....18

16 SEM micrograph of reaction products from Beulah lignite.....19

17 Conceptual schematic of the SCR reactor slipstream field test unit 20

18 SCR catalyst section.....20

Continued. . .

LIST OF FIGURES (continued)

19 Haldor Topsoe SCR catalyst showing the gas flow passages 21

20 Babcock Hitachi SCR catalyst showing the gas flow passages 22

21 Catalyst pressure drop at Baldwin Station at 0 to 2 months of operation 24

22 Catalyst pressure drop at Baldwin Station at 2 to 4 months of operation 24

23 Catalyst pressure drop at Baldwin Station at 4 to 6 months of operation 25

24 Catalyst pressure drop at Columbia Station at 0 to 2 months of operation 25

25 Catalyst pressure drop at Columbia Station at 2 to 4 months of operation 26

26 Catalyst pressure drop at Columbia Station at 4 to 6 months of operation 26

27 Catalyst pressure drop at Coyote Station at 0 to 2 months of operation 27

28 Catalyst pressure drop at Coyote Station at 2 to 4 months of operation 28

29 Catalyst pressure drop at Coyote Station at 4 to 6 months of operation 28

30 Pictures of catalyst inlet after about 2 months of testing at each plant 30

31 Pictures of catalyst inlet after about 4 months of exposure to flue gas and particulate 31

32 SEM images of ash collected on catalyst surface at the Baldwin Station after 2 months of exposure 32

33 SEM images of ash collected on catalyst surface at the Baldwin Station after 4 months of exposure 34

34 SEM images of ash collected on catalyst surface at the Baldwin Station after 6 months of exposure 36

35 SEM images of ash collected on catalyst surface at the Columbia Station after 2 months of exposure 38

36 SEM images of ash collected on catalyst surface at the Columbia Station after 4 months of exposure 40

Continued. . .

LIST OF FIGURES (continued)

37 SEM images of ash collected on catalyst surface at the Columbia Station after 6 months of exposure 42

38 SEM images of ash collected on catalyst surface at the Coyote Station after 2 months of exposure 44

39 SEM images of ash collected on catalyst surface at the Coyote Station after 4 months of exposure 46

40 SEM images of ash collected on catalyst surface at the Coyote Station after 6 months of exposure 48

41 X-ray diffraction of ash collected on SCR catalyst 50

42 Simplified illustration of ash partitioning in combustion systems 50

43 Comparison of entrained ash and deposited ash on catalyst for Columbia Station 51

44 Mechanism of SCR catalyst blinding via the formation of sulfates and carbonates 52

45 Mercury speciation measurement at the inlet and outlet of the SCR catalyst upon installation of the catalyst 53

46 Mercury speciation measurement at the inlet and outlet of the SCR catalyst after exposure to flue gas and particulate for 4 months 53

47 Mercury speciation measurement at the inlet and outlet of the SCR catalyst after exposure to flue gas and particulate for 2 months 54

48 Mercury speciation measurement at the inlet and outlet of the SCR catalyst after exposure to flue gas and particulate for 6 months 54

LIST OF TABLES

1 Flue Gas Makeup 3

2 Description of Power Plants Tested 5

3 Key Selection Criteria 5

4 Ultimate Analysis Results 6

5 Ash Composition 6

6 CCSEM Analysis Results for Beulah, Antelope, and Caballo 7

7 Composition of Coal Ashes Used in Bench-Scale Testing 9

8 SEM/Energy-Dispersive Spectroscopy Analysis Results from Nanticoke PRB at 800°F ...17

9 SEM/EDS Analysis Results from Nanticoke PRB–LSUS blend at 800°F 18

10 SEM/EDS Analysis Results from Beulah Lignite at 800°F 19

11 Selected Operating Conditions of the SCR Catalysts 23

12 Chemical Composition of Selected Points and Areas in Figure 32 33

13 Chemical Composition of Selected Points and Areas in Figure 33 35

14 Chemical Composition of Selected Points and Areas in Figure 34 37

15 Chemical Composition of Selected Points and Areas in Figure 35 39

16 Chemical Composition of Selected Points and Areas in Figure 36 41

17 Chemical Composition of Selected Points and Areas in Figure 37 43

18 Chemical Composition of Selected Points and Areas in Figure 38c 45

19 Chemical Composition of Selected Points and Areas in Figure 39b and 39c 47

20 Chemical Composition of Selected Points and Areas in Figure 40 49

21 Results of Reactivity Tests for the Baldwin Station 49

JV 31 – EVALUATION OF POTENTIAL SCR CATALYST BLINDING DURING COAL COMBUSTION AND ADD-ON: IMPACT OF SCR CATALYST ON MERCURY OXIDATION IN LIGNITE-FIRED COMBUSTION SYSTEMS

EXECUTIVE SUMMARY

The goal of this project by the Energy & Environmental Research Center (EERC) is to determine the potential of low-rank coal ash to cause blinding or masking of selective catalytic reduction (SCR) catalysts. The primary goal of the add-on is to determine the effects of new and aged catalyst on the oxidation of mercury at full-scale power plants.

Two SCR slipstream reactors were constructed to accomplish the goals of this project. The test chambers are approximately 19 cm (7.5 inches) square and are able to accommodate catalyst sections up to 1 meter (3.3 feet) in length. The chambers are electrically heated and fully instrumented to limit heat loss and to maintain a catalyst face velocity of 5 m/s (16.4 ft/s).

The SCR reactors were installed at three different plant locations and operated until the catalyst had 6 months of operating time. The units that were chosen for this study are the Columbia Station (pulverized coal-fired), the Baldwin Station (cyclone-fired), and the Coyote Station (cyclone-fired). The Coyote Station fires North Dakota lignite, while the other two stations burn Powder River Basin (PRB) coal. The catalyst was sampled every 2 months and analyzed with scanning electron microscopy (SEM).

Bench-scale and Facility for Analysis of Chemical Thermodynamics (FACT) modeling studies were also conducted in the laboratory prior to the reactors being installed at the host utilities. Experiments were carried out in a thermogravimetric analyzer (TGA) system at 315°C (600°F), 370°C (700°F), and 427°C (800°F) with simulated flue gas. Ash samples created from the test coals were placed on the TGA pan with and without catalyst. The rate of sample weight gain was then monitored. The ash was then analyzed with SEM techniques to identify the species that were present.

The results of the bench-scale analysis indicate that the rate of weight gain increases with increasing temperature, and calcium sulfates were the predominant species formed. The rate of sulfate formation could increase as much as tenfold with the addition of catalyst to the system. Low-sulfur bituminous and PRB blends exhibited a higher rate of sulfate formation and, therefore, would have a higher blinding potential than a 100% PRB or lignite. Results of the FACT modeling indicate that there is a high potential to form alkali and alkaline-earth sulfates, carbonates, and phosphates while SCRs are operated at utilities burning lignite and PRB coals.

The data collected during the three slipstream reactor tests indicate that the pressure drop across the catalyst was found to be the most significant for the lignite-fired plant as compared to the subbituminous-fired plants. Both lignite and PRB coals had significant accumulations of ash on the catalyst, on both macroscopic and microscopic levels. On a macroscopic level, there were significant observable accumulations that plugged the entrance as well as the exit of the catalyst

sections. On a microscopic level, the ash materials filled pores in the catalyst and, in many cases, completely masked the pores within 4 months of operation.

The deposits on the surfaces and within the pores of the catalyst consisted of mainly alkali and alkaline-earth element-rich phases that have been sulfated. The mechanism for the formation of the sulfate materials involves the formation of very small particles rich in alkali and alkaline-earth elements, transport of the particles to the surface of the catalyst, and reactions with SO_2/ SO_3 to form sulfates. X-ray diffraction analysis identified $CaSO_4$ as a major phase and $Ca_3Mg(SiO_4)_2$ and $CaCO_3$ as minor phases.

Lignite and subbituminous coals contain high levels of organically associated alkali and alkaline-earth elements, including sodium, magnesium, calcium, and potassium in addition to mineral phases. During combustion, the inorganic components in the coal are partitioned into various size fractions based on the type of inorganic component and their association in the coal and combustion system design and operating conditions. The results of this testing found that the smaller size fractions of ash are dominated by partially sulfated alkali and alkaline-earth elements. The composition of the size fractions was compared to the chemical composition of the ash deposited on and in the catalyst. The comparison shows that the composition of the particle captured in the SCR catalyst is very similar to the <5-µm size fraction.

This study suggests the careful evaluation of each SCR installation on applications using subbituminous and lignite coals. Improvements are needed to ensure technical feasibility, especially with lignite-fired units. Installations involving lignite fuels will need advanced cleaning techniques to handle the high sodium and high dust loads associated with burning most lignite fuels.

The ability of mercury to be oxidized across the SCR catalyst was investigated at the Coyote Station. The Coyote Station is fired on North Dakota lignite, and the flue gases are dominated by elemental mercury. Measurement of mercury speciation was conducted using the Ontario Hydro (American Society for Testing and Materials D6784-02) method at the inlet and the outlet of the SCR reactor. These results show limited oxidation of mercury across the SCR catalyst when lignite coals are fired. The reasons for the lack of mercury oxidation include the following: no chlorine present in the coal and flue gas to catalytically enhance the oxidation of Hg^0, higher levels of alkali and alkaline-earth elements acting as sorbents for any chlorine present in the flue gas, and lower levels of acid gases present in the flue gas.

JV 31 – EVALUATION OF POTENTIAL SCR CATALYST BLINDING DURING COAL COMBUSTION AND ADD-ON: IMPACT OF SCR CATALYST ON MERCURY OXIDATION IN LIGNITE-FIRED COMBUSTION SYSTEMS

INTRODUCTION

The Energy & Environmental Research Center (EERC) investigated selective catalytic reduction (SCR) for NO_x control and mercury oxidation using a slipstream reactor at power plants firing subbituminous and lignite coals to determine the potential for ash plugging and blinding and mercury oxidation. SCR units lower NO_x emissions by reducing NO_x to N_2 and H_2O. Ammonia (NH_3) is the most common reducing agent used for the SCR of NO_x. The SCR process involves the use of a metal oxide catalyst such as titanium dioxide (TiO_2)-supported vanadium pentoxide (V_2O_5). These units are operated at about 340°–370°C (650°–700°F). Subbituminous and lignitic coals are known for their ability to produce alkali and alkaline-earth sulfate-bonded deposits at low temperature (<1000°C) in utility boilers. The mechanisms of the formation of low-temperature sulfates have been extensively examined and modeled by the EERC in work termed Project Sodium and Project Calcium in the early 1990s (1, 2). Deposit buildup of this type blinds or masks the catalyst, diminishing its reactivity for converting NO_x to N_2 and water and potentially creating increased NH_3 slip (3). Elemental mercury oxidation has been observed in laboratory-, pilot-, and full-scale testing using SCR catalysts (4–6). In these studies, the metal oxides, V_2O_5 and TiO_2, have been shown to promote the conversion of elemental mercury to oxidized and/or particulate-bound mercury. Full-scale tests in Europe (7) and the United States (8) have indicated that the V_2O_5 and TiO_2 catalyst may promote the formation of oxidized mercury. The ability to oxidize mercury is largely dependent on the composition of the coal (8).

Lignite and subbituminous coals produce ash that plug and blind catalysts (9–12). The problems currently being experienced on SCR catalysts include the formation of sulfate- and phosphate-based blinding materials on the surface of catalysts and the carrying of deposit fragments, or popcorn ash, from other parts of the boiler and depositing them on top of the SCR catalysts (3). The most significant problem that limits the successful application of SCR catalysts to lignite coal is the formation of low-temperature sodium–calcium–magnesium sulfates, phosphates and, possibly, carbonates on the surfaces of catalysts and the carryover of deposits that will plug the catalyst openings, resulting in increased pressure drop and decreased efficiency (3, 11–14). The degree of the ash-related impacts on SCR catalyst performance depends upon the composition of the coal, the type of firing systems, flue gas temperature, and catalyst design (11, 12, 14, 15).

Licata and others (13) conducted tests on a South African and a German Ruhr Valley coal and found that the German Ruhr Valley coal significantly increased the pressure drop across the catalyst because of the accumulation of ash. They found that the German coal produced a highly adhesive ash consisting of alkali (K and Na) sulfates. In addition, they reported that the alkali elements are in a water-soluble form and highly mobile and will migrate throughout the catalyst material, reducing active sites. The water-soluble form is typical of organically associated alkali elements in coals. The German Ruhr Valley coal has about 9.5% ash and 0.9% S on an as-

received basis, and the ash consists mainly of Si (38.9%), Al (23.2%), Fe (11.6%), and Ca (9.7%), with lower levels of K (1.85%) and Na (0.85%) (13). Cichanosicz and Muzio (14) summarized the experience in Japan and Germany and indicated that the alkali elements (K and Na) reduced the acidity of the catalyst sites for total alkali content (K + Na + Ca + Mg) of 8%–15% of the ash in European power plants. Licata et al. also found that alkaline-earth elements such as calcium react with SO_3 on the catalyst, resulting in plugging of pores and a decrease in the ability of NH_3 to bond to catalyst sites. The levels of calcium in the coals that caused blinding ranged from 3% to 5% of the ash. Studies conducted on the impact of alkali elements associated with biomass found that, when biomass is fired, poisoning and blinding of SCR catalysts occurred (16, 17).

This study took a three-pronged approach to solve the issues involving low-rank fuels and the SCR catalyst. Studies were conducted at both the pilot and bench scales and were compared to a thermodynamic equilibrium model. In order to facilitate the pilot-scale study, two slipstream SCR systems were constructed. The slipstream reactors were installed at three power plants. Two of the plants were cyclone-fired: one with lignite and one with subbituminous coal. The third plant was a pulverized-coal (pc), tangentially fired unit using subbituminous coal. The slipstream reactors were designed to expose SCR catalysts to flue gas and particulate matter under conditions that simulate gas velocities, temperatures, and NH_3 injection of a full-scale pilot plant. The control system maintains catalyst temperature, pulse air to remove accumulated deposits, and a constant gas flow across the catalyst; it logs pressure drops and temperatures. The reactor was operated in an automated mode and could be remotely controlled via modem. Testing at each power plant was conducted over 6 months. The reactor was inspected and cleaned at 2-month intervals, and a catalyst section was removed for analysis. The catalysts and associated ash deposits were analyzed to determine the characteristics of the ash on the surface and in the pores. In addition, mercury speciation in the flue gas upstream and downstream of the catalyst was conducted at 2-month intervals during the testing at the lignite-fired plant. The ability of the SCR catalyst to catalyze gaseous elemental mercury (Hg^0[g]) to more soluble and chemically reactive $Hg^{2+}X$(g) forms was evaluated, along with the potential increase in particle-associated mercury (Hg[p]). Increasing the oxidized and particulate fractions of mercury has the potential to increase the efficiency of mercury capture by conventional control devices such as wet flue gas desulfurization scrubbers and electrostatic precipitators.

EXPERIMENTAL

Thermochemical Equilibrium Modeling

The Facility for the Analysis of Chemical Thermodynamics (FACT) is a digital thermodynamic equilibrium model that assesses fuel quality effects on ash behavior in a boiler. It predicts molar fractions (partial pressures) of all gas, liquid, and solid stable components in a system by using the principle of Gibbs free energy minimization. FACT output includes quantities, compositions, and viscosities of liquid and solid mineral phases; the model accurately predicts the behavior of fuel ash, including biomass-derived ash, for different boiler temperature regimes.

In this study, the bulk ash composition and the atmosphere used in the thermogravimetric analyzer (TGA) testing were input to the FACT model. In this model, each reaction is considered independent of all other reactions. For example, the FACT model may predict that species X will dominate while the empirical results show that species Y tends to form (i.e., selectivity and kinetics are not considered by the model).

Bench-Scale TGA Study

Fuels were first combusted in the EERC's conversion and environmental process simulator. Ash resulting from the combustion of these fuels was collected and size-fractionated. Tests were carried out on the size-fractionated ash in a TGA under atmospheric conditions that mimic a combustion environment. The simulated flue gas atmosphere consisted of CO_2, SO_2, NH_3, N_2, O_2, H_2O, and P_2O_5. The flue gas makeup is presented in Table 1. The weight gain of the ash or ash–catalyst mixtures was measured as a function of time and temperature. The tests were conducted at 316°, 371°, and 427°C (600°, 700°, and 800°F). The resulting mixtures were analyzed to determine the influence of SCR catalysts on ash behavior.

Table 1. Flue Gas Makeup

N_2	74%
H_2O	8%
CO_2	14%
O_2	4%
NH_3	100–300 ppm
SO_2	0.04%
P	1–1000 ppm

Slipstream Reactor Installation and Operation

Upon installation at each utility boiler unit, flue gas temperature, composition, and velocity measurements were obtained using portable equipment. Shakedown testing of the unit was conducted to ensure that all components were operating properly and that data were being logged and could be retrieved. After installation and shakedown were completed, the reactor was operated in a computer-controlled, automated mode and monitored on a daily basis to ensure proper operation and data quality. During operation of the SCR slipstream system, catalyst temperature, sootblowing frequency, and pressure drop across the catalyst were monitored and logged. Samples of the exposed SCR catalyst and associated deposits were obtained after exposure to flue gas and particulate for 2, 4, and 6 months. The samples of the catalyst were analyzed to determine the components that were bonding and filling pores, resulting in decreased reactivity.

SEM Ash Characterization

The characteristics of the ash that accumulated on the catalyst were examined using scanning electron microscopy (SEM)–x-ray microanalysis and x-ray diffraction (XRD) (18). The

samples were either placed on double-stick tape for surface analysis or mounted in epoxy for cross-section analysis. Correlations between the physical and chemical characteristics of any ash deposits on the SCR test section and entrained-ash sample collected at the chamber inlet and the coal inorganic composition will be made to discern mechanisms of SCR blinding. Entrained ash was collected at the Columbia Station only and characterized with respect to composition and size.

Mercury Measurement

At the Coyote Station, the Ontario Hydro (OH) mercury speciation sampling train was used to determine mercury forms across the SCR test section. The OH extractive mercury speciation sampling technique was used to measure potential mercury conversion across the SCR system over a period of several hours after fresh installation of the SCR test chamber and again just prior to removal of SCR catalyst sections.

The procedure used to conduct the mercury speciation sampling was American Society for Testing and Materials Method D6784-02 entitled "Standard Test Method for Elemental, Oxidized, Particle-Bound and Total Mercury in Flue Gas Generated from Coal-Fired Stationary Sources (Ontario Hydro method)" (19).

The OH method follows standard U.S. Environmental Protection Agency (EPA) methods for isokinetic flue gas sampling (EPA Methods 1–3 and EPA Method 5/17). A sample is withdrawn from the flue gas stream isokinetically through the filtration system, which is followed by a series of impingers in an ice bath. Particulate-bound mercury is collected on the filter; Hg^{2+} is collected in impingers containing 1 N potassium chloride solution; and elemental mercury is collected in one impinger containing a 5% nitric acid and 10% peroxide solution and in three impingers containing a solution of 10% sulfuric acid and 4% potassium permanganate. An impinger containing silica gel collects any remaining moisture. The filter media is quartz fiber filters. The filter holder is glass or Teflon-coated. An approximate 2-hour sampling time was used, with a target sample volume of 1 standard cubic meter.

RESULTS AND DISCUSSION

Task 1 – Identification of Test Coals and Utility Host Sites

Three host utility sites were chosen for the installation of the SCR reactors. The utilities were chosen based on their ability to provide all of the necessary support and hardware for the operation of the SCR reactors. The electric utility units selected for testing are shown in Table 2. The plants where the SCR slipstream system was installed included Alliant Energy's Columbia Station, Dynegy's Baldwin Station, and Otter Tail Power Company's Coyote Station.

Table 2 describes the plants, and Table 3 summarizes the characteristics and selection criteria. The selection criteria that were most important to the success of this project were geographic location, a base load plant, and a consistent supply of one fuel for the duration of the study.

Table 2. Description of Power Plants Tested

	Baldwin	Columbia	Coyote
Unit No.	1	2	1
Utility	Dynegy	Alliant	Otter Tail
Boiler Type	Cyclone	T-fired	Cyclone
Fuel type	Antelope – subbituminous	Caballo – subbituminous	Beulah – Zap lignite
Load	Base	Base	Base
Location	Baldwin, IL	Portage, WI	Beulah, ND
MW	600	520	425

Table 3. Key Selection Criteria

Field Test 1 – Columbia Station

- Tangentially fired boiler to show differences in ash partitioning as compared to cyclone-fired systems.
- High-potential-blinding coal in Caballo, which can be burned nearly 100% for the entire test.

Field Test 2 – Baldwin Station

- Plant is cyclone fired.
- Units already are equipped to do slipstream testing.
- Plant currently fires a blend of Antelope coal and tires; plant is willing to fire 100% Antelope.
- High-potential-blinding coal in Antelope.

Field Test 3 – Coyote Station

- Cyclone-fired with lignite.
- High-potential-blinding coal with high alkali and alkaline-earth elements. Coal can have very high sodium content and is known to cause significant low-temperature deposition.

The units tested were selected based on the fuels fired, boiler type, and availability of the unit for sampling. The average composition of the coals fired during the testing is listed in Tables 4 and 5. The subbituminous coals were typically low ash, nominally 4.5%–5.5% with very high levels of calcium in the ash. In comparison, the lignite contains higher levels of ash and lower calcium but higher levels of sodium. The alkali and alkaline-earth elements are primarily associated with the organic matrix of the coal as salts of carboxylic acid groups (18). The portion of the ash-forming components that are associated with the organic matrix of the coal for subbituminous coal ranges from 30% to 60% (18); for the lignite coal, the portion is about 20% to 40%. The remaining ash-forming components consist of mineral grains. For these coals, the percentage organically associated is 29% for the Antelope, 36% for Caballo, and 19% for Beulah. The minerals present in the coals as determined by computer-controlled scanning electron microscopy (CCSEM) analyses are listed in Table 6. The primary minerals present in the subbituminous coals include quartz and various clay minerals with some pyrite and a mineral that is rich in Ca, Al, and P. This mineral has been identified in some coals as crandalite. The primary minerals found in the Beulah coal include clay minerals (kaolinite), pyrite, and quartz.

Table 4. Ultimate Analysis Results (dry basis), wt%

	Antelope	Caballo	Beulah
Ash Content	7.28	6.59	11.62
Total Sulfur	0.33	0.51	1.49
Carbon	69.97	67.88	61.50
Hydrogen	4.77	4.83	3.96
Nitrogen	1.05	1.24	1.08
Oxygen (by difference)	16.61	18.96	20.35

Table 5. Ash Composition (wt% equivalent oxide)

Oxide	Antelope	Caballo	Beulah
SiO_2	24.82	26.70	16.50
Al_2O_3	13.55	16.60	13.30
TiO_2	1.39	1.10	0.80
Fe_2O_3	7.52	5.10	16.60
CaO	26.68	25.10	19.50
MgO	7.14	8.00	7.40
K_2O	0.17	0.30	0.20
Na_2O	1.47	1.00	5.20
P_2O_5	0.90	1.70	0.00
SO_3	16.33	14.40	19.80

Task 2 – Bench-Scale Testing and FACT Modeling

Bench-Scale Testing

The goal of the bench-scale testing was to determine the effect catalyst would have on the conversion of SO_2 to SO_3 and the resulting increase in catalyst blinding. Tests were conducted with and without catalyst on the following fuels: Nanticoke Powder River Basin (PRB), Beulah lignite, and Nanticoke PRB and a low-sulfur U.S. (LSUS) bituminous blend.

The results of the study indicate that the addition of the catalyst to the ash and increased temperature increased the rate of weight gain by as much as tenfold. The weight gain can be directly linked to the rate of sulfation. The test results in Figures 1–3 were compiled using the gas concentrations noted in Table 1 minus the NH_3 and phosphorus compounds (baseline tests). Table 7 contains the ash analysis of the coals used in the bench-scale testing. Figure 1 contains the weight gain curves for the Nanticoke PRB test. The rate of weight gain increased as the temperature increased from 316° to 427°C (600° to 800°F).

Figure 2 contains the weight gain curve for the Beulah lignite. Again the weight gain increased as the temperature was increased from 316° to 427°C (600° to 800°F). The rate of weight gain was similar to what was seen with the Nanticoke PRB test.

Table 6. CCSEM Analysis Results for Beulah, Antelope, and Caballo (values are wt% on a mineral basis)

	Caballo	Antelope	Beulah
Total Mineral wt% on a Coal Basis:	2.8	3.2	8.4
Quartz	40.4	31.5	11.0
Iron Oxide	0.0	2.4	4.4
Periclase	0.0	0.0	0.0
Rutile	2.4	0.3	0.0
Alumina	0.0	0.0	1.1
Calcite	0.0	0.4	0.1
Dolomite	0.0	0.5	0.0
Ankerite	0.0	0.0	0.2
Kaolinite	23.7	17.1	4.9
Montmorillonite	0.4	6.5	6.6
K Al-Silicate	0.0	1.6	7.2
Fe Al-Silicate	0.0	0.8	9.0
Ca Al-Silicate	0.1	1.0	2.6
Na Al-Silicate	0.0	0.0	0.1
Aluminosilicate	0.7	3.3	3.2
Mixed Al-Silicate	0.0	1.0	5.5
Fe Silicate	0.0	0.0	0.0
Ca Silicate	0.0	0.4	0.0
Ca Aluminate	0.0	0.0	0.0
Pyrite	16.2	0.0	0.8
Pyrrhotite	0.0	4.8	18.4
Oxidized Pyrrhotite	0.0	0.5	0.5
Gypsum	0.4	0.0	0.5
Barite	0.8	0.5	3.0
Apatite	0.0	0.2	0.0
Ca Al-P	8.5	13.5	0.1
KCl	0.0	0.0	0.0
Gypsum/Barite	0.0	0.1	0.0
Gypsum/Al-Silicate	0.1	0.9	4.0
Si-Rich	0.3	3.7	4.9
Ca-Rich	0.0	0.0	0.0
Ca-Si-Rich	0.0	0.1	0.0
Unclassified	3.2	8.7	11.9
Totals	100.0	100.0	100.0

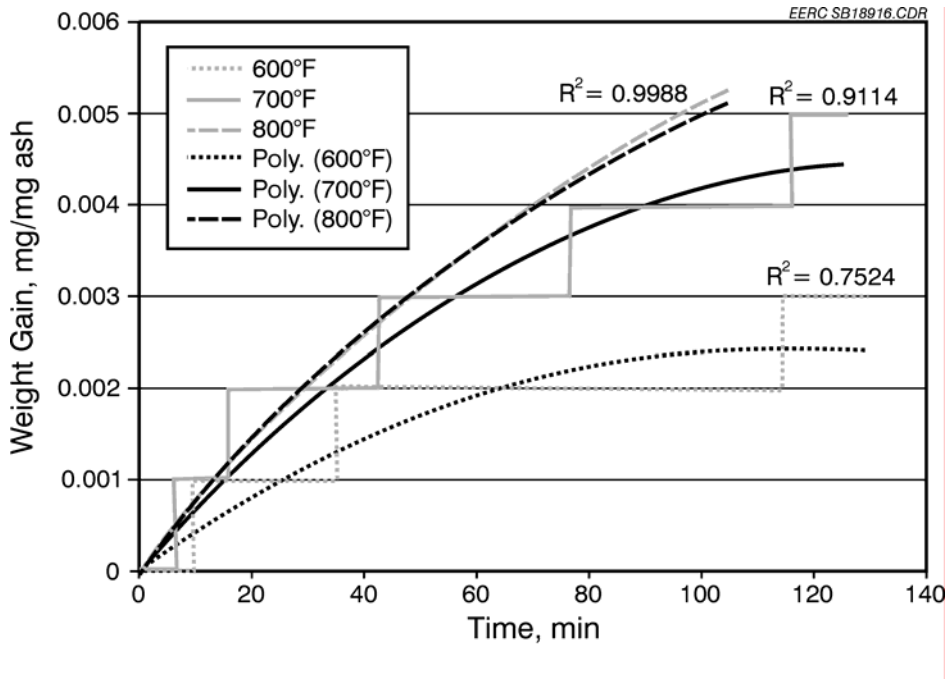

Figure 1. Weight gain curves for Nanticoke PRB (less than 3 µm), no catalyst.

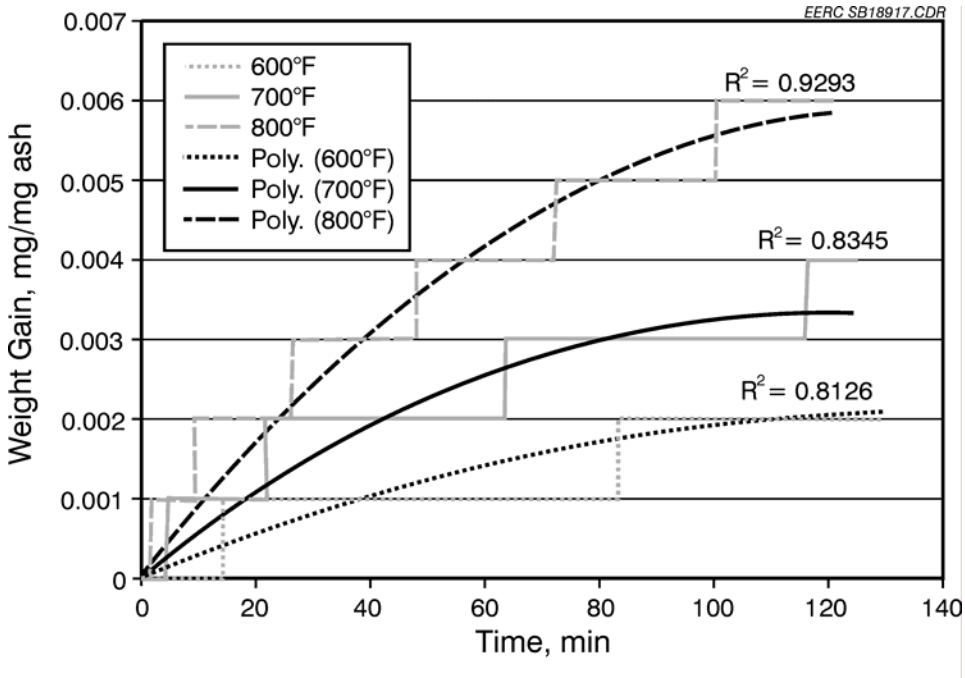

Figure 2. Weight gain curves for Beulah lignite (less than 3 µm), no catalyst.

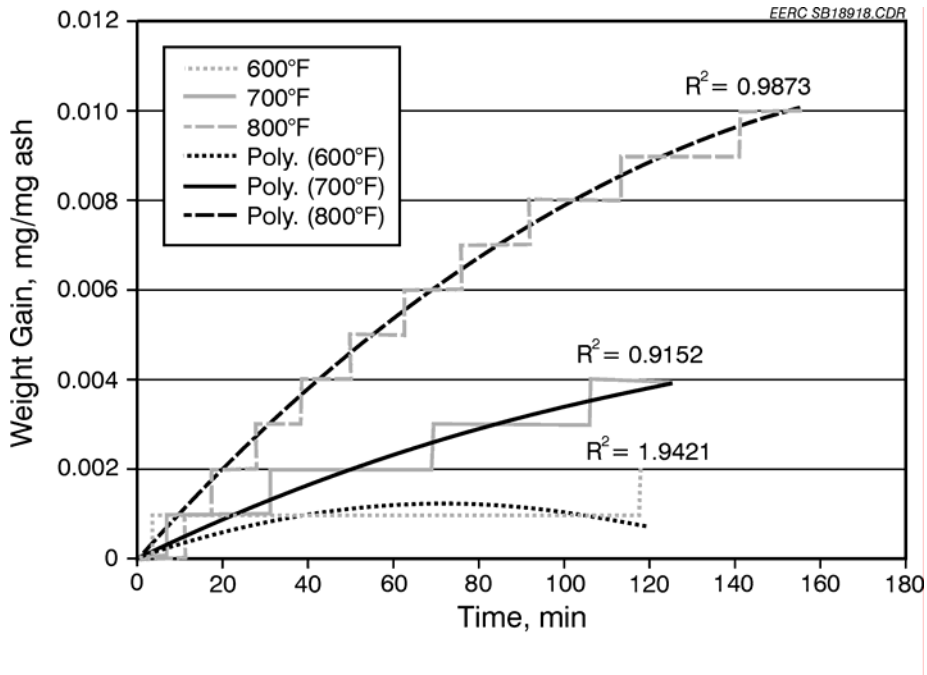

Figure 3. Weight gain curves for Nanticoke PRB–LSUS blend (less than 3 µm), no catalyst.

Table 7. Composition of Coal Ashes Used in Bench-Scale Testing

	Nanticoke 100% PRB		Nanticoke 52% PRB–48% LSUS		Beulah	
Oxides, wt%	(a)[1]	(b)[2]	(a)	(b)	(a)	(b)
SiO_2	27.9	32.0	43.4	48.4	31.5	39.7
Al_2O_3	17.7	20.3	26.7	29.7	14.2	17.9
Fe_2O_3	6.2	7.1	4.8	5.3	7.3	9.2
TiO_2	1.5	1.8	1.6	1.8	0.8	1.0
P_2O_5	1.0	1.2	0.4	0.4	0.2	0.2
CaO	24.8	28.5	8.5	9.4	15.8	19.9
MgO	6.6	7.6	2.6	2.9	5.8	7.3
Na_2O	1.0	1.2	0.7	0.7	3.1	3.9
K_2O	0.4	0.5	1.2	1.3	0.8	1.0
SO_3	12.9	—	10.2	—	20.6	—

[1] Oxide concentrations normalized to a closure of 100%.
[2] Oxide concentrations renormalized to an SO_3-free basis.

A blend of the Nanticoke PRB and an LSUS bituminous coal was tested at a 52–48 blend (PRB–LSUS). The weight gain curves for this test are in Figure 3. The results of this experiment are again similar to those obtained in the previous two cases, with the exception of the 427°C (800°F) test. The 427°C (800°F) test in this case gains slightly more weight than the previous two experiments. At high temperatures, this blend had almost double the weight gain from the

straight PRB case. This indicates that there is likely more sulfur available from the bituminous coal.

More testing was completed on the Nanticoke PRB and the PRB–LSUS blend. In Figures 4–5, the gas used in the study now contains the NH_3 and phosphorus compounds in addition to the gas used in the previous three tests. Figure 4 contains the data for the Nanticoke PRB test with NH_3 and phosphorus. The addition of the NH_3 and phosphorus compounds increased the rate of weight gain in the 427°C (800°F) test. The difference in rates as temperature was increased became less pronounced.

Figure 5 contains the weight gain curves for the PRB–LSUS test. The rate of weight gain was also increased; however, the temperature effect was still present (increased weight gain with increased temperature).

The baseline tests (without NH_3 and phosphorus compounds) were repeated with the addition of SCR catalyst to the mixture. The results of these tests are in Figures 6–7. Figure 6 contains the weight gain curves for the Nanticoke PRB test with catalyst and the Nanticoke PRB test at baseline conditions and 427°C (800°F). The rate of weight gain with the addition of catalyst at 427°C (800°F) increased approximately 7-fold in this case. The addition of the catalyst will increase the amount of SO_2 that is oxidized to a more reactive form (SO_3), which will in turn increase the rate of sulfate formation.

Figure 7 contains the weight gain curves for the PRB–LSUS blend with catalyst. In this test, the rate of weight gain increased almost tenfold. Again, the increased rate can be attributed to more SO_3 in the system.

FACT Modeling

FACT thermodynamic equilibrium modeling was conducted on each of the ash and flue gas systems tested in the bench-scale screening. The FACT modeling will give an indication of what chemical species are thermodynamically favored at the temperature present in the SCR. Figures 8–13 contain the results of the FACT modeling on the Nanticoke PRB, Beulah lignite, and the Nanticoke PRB–LSUS blend. The gas composition used for the modeling is the same as what was used for the bench-scale analysis in Table 1.

Figures 8–10 have the results for the Nanticoke PRB, Nanticoke PRB–LSUS blend, and the Beulah lignite with 300 ppm NH_3 and 1000 ppm phosphorus pentoxide added. The model predicts that in all three cases the alkali/alkaline-earth phosphates and sulfates will be the predominant species formed. Trace amounts of phosphoric and sulfuric acid will also be present at lower temperatures (232°C [450°F]).

Figures 11–13 have the results for the Nanticoke PRB, the Nanticoke PRB–LSUS blend, and the Beulah lignite with 100 ppm NH_3 and 1 ppm phosphorus pentoxide added. With less phosphorus present, the model predicts that sulfates will dominate. In the case of the Nanticoke PRB, the formation of carbonate compounds is also predicted.

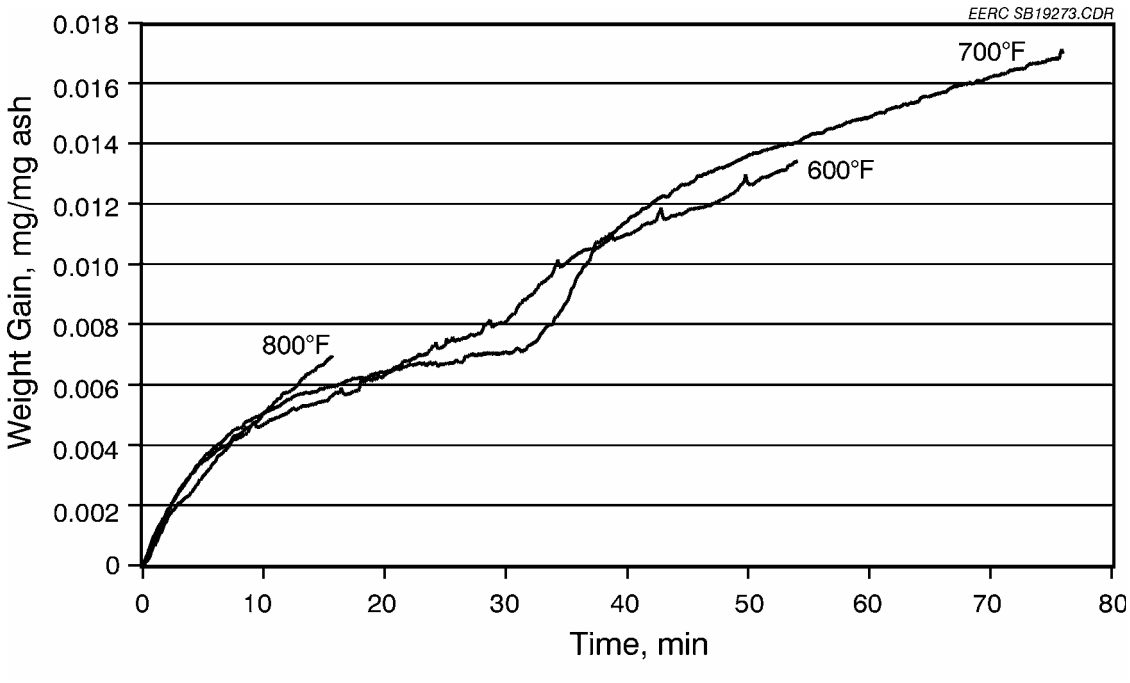

Figure 4. Weight gain curves for Nanticoke PRB (less than 3 µm) with ammonia and phosphorus compounds, no catalyst.

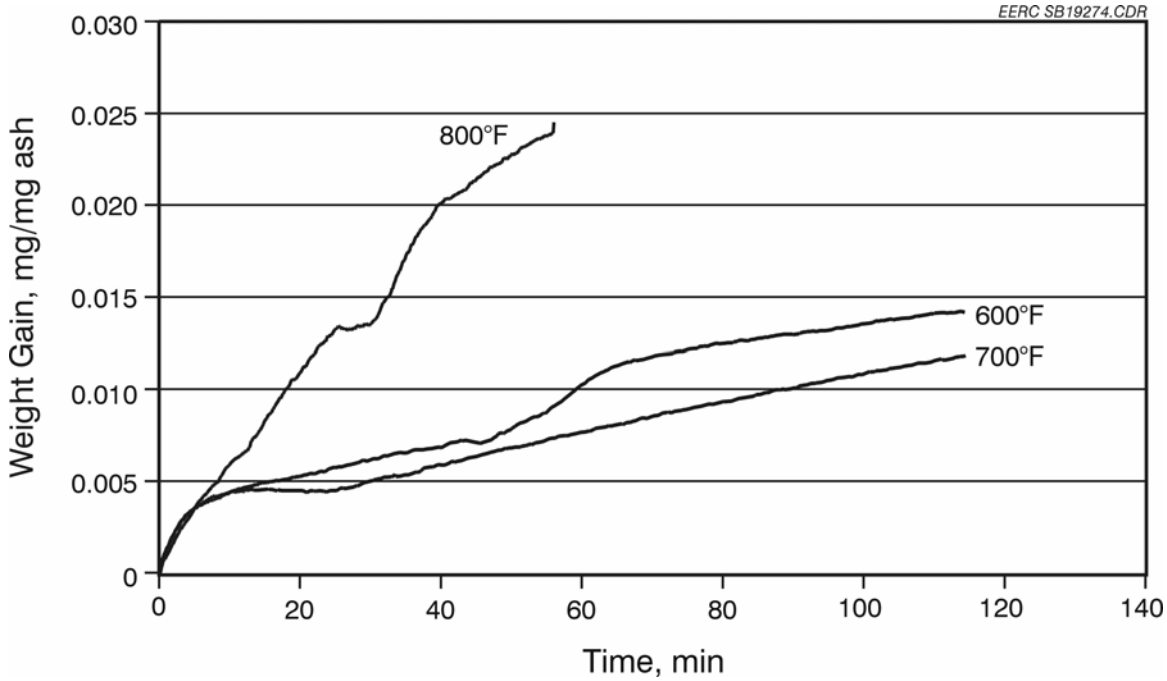

Figure 5. Weight gain curves for Nanticoke PRB–LSUS blend (less than 3 µm) with ammonia and phosphorus compounds, no catalyst.

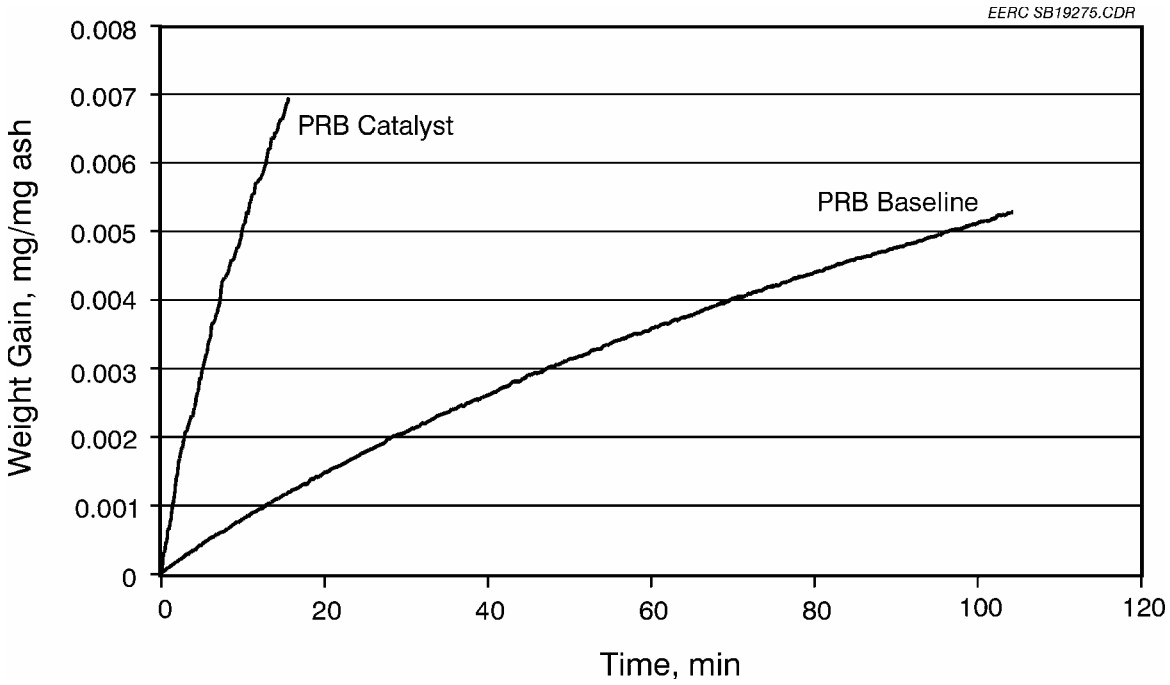

Figure 6. Weight gain curves for baseline Nanticoke PRB and Nanticoke PRB with catalyst.

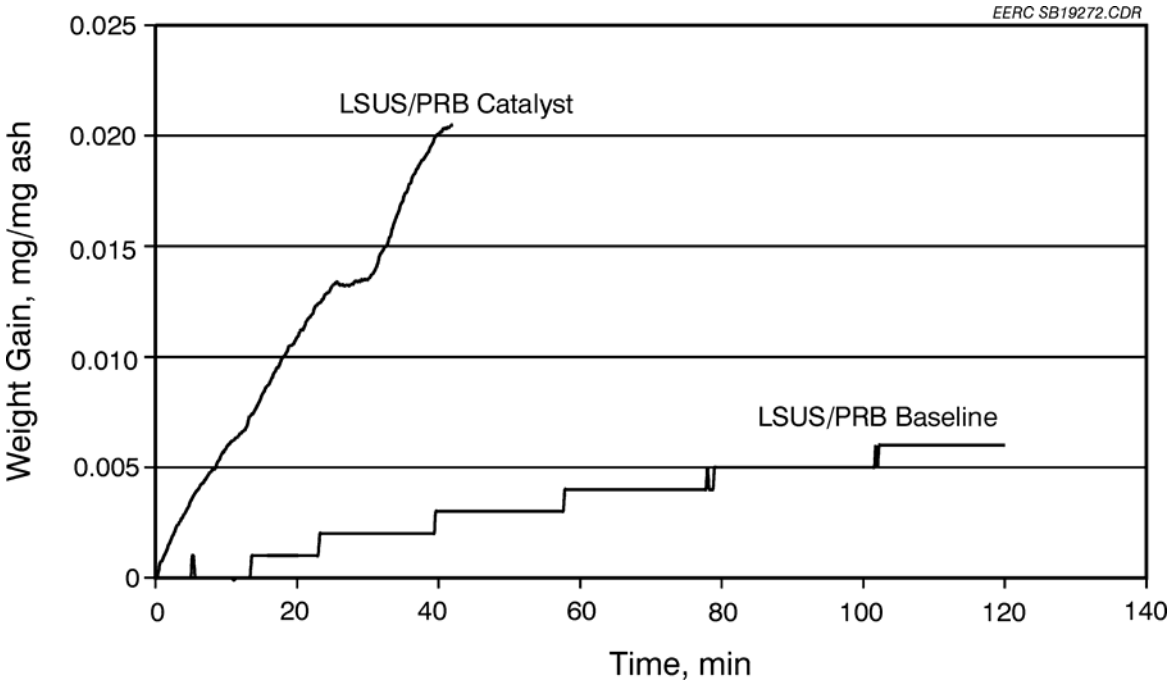

Figure 7. Weight gain curves for baseline LSUS–Nanticoke PRB blend and LSUS–Nanticoke PRB blend with catalyst.

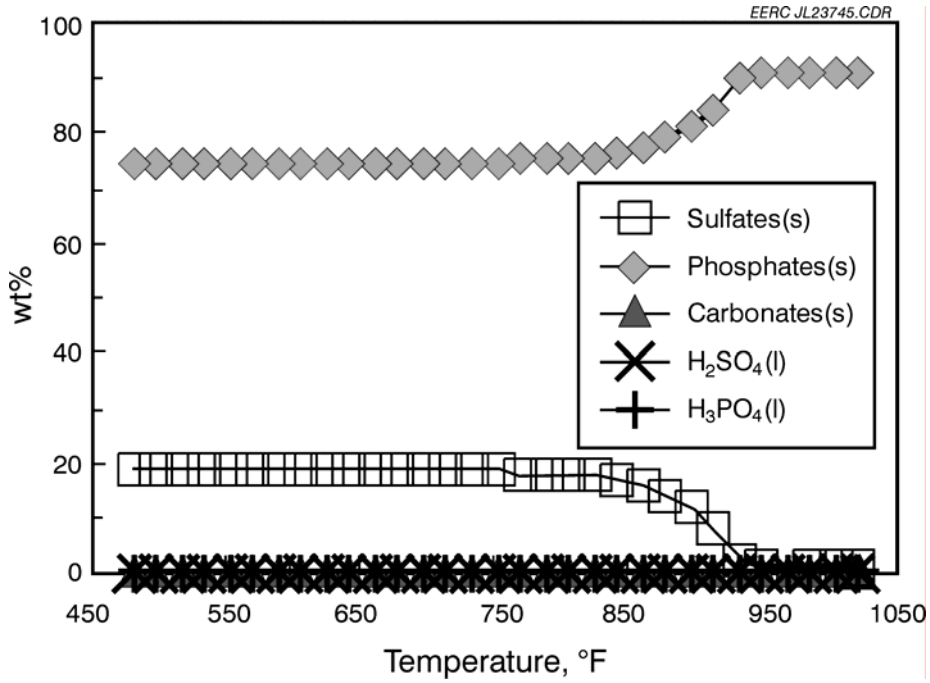

Figure 8. FACT modeling results for Nanticoke PRB with 300 ppm ammonia and 1000 ppm P_2O_5.

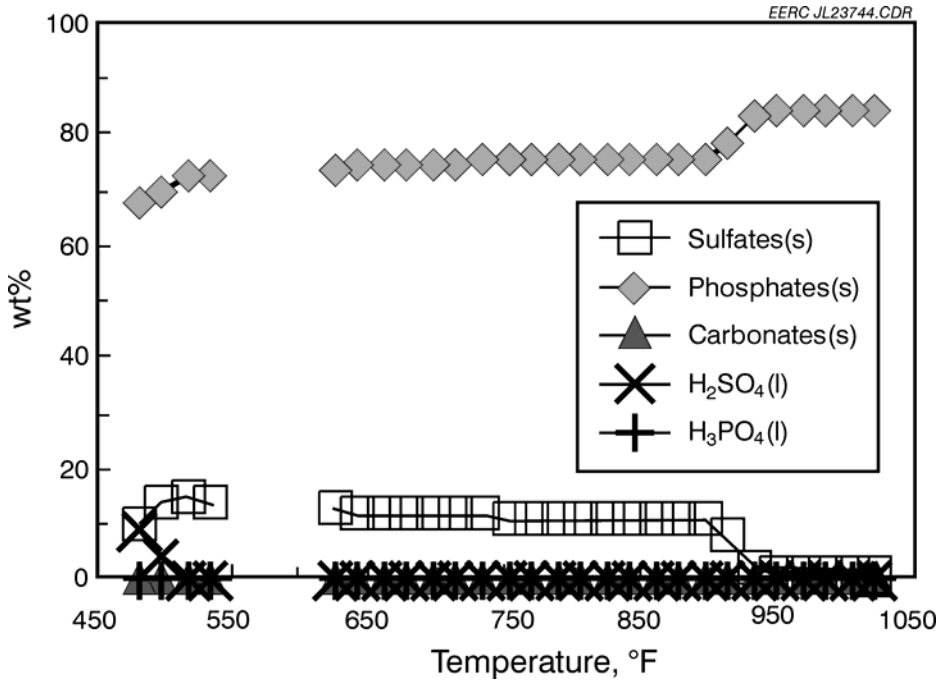

Figure 9. FACT modeling results for Nanticoke PRB–LSUS blend with 300 ppm ammonia and 1000 ppm P_2O_5.

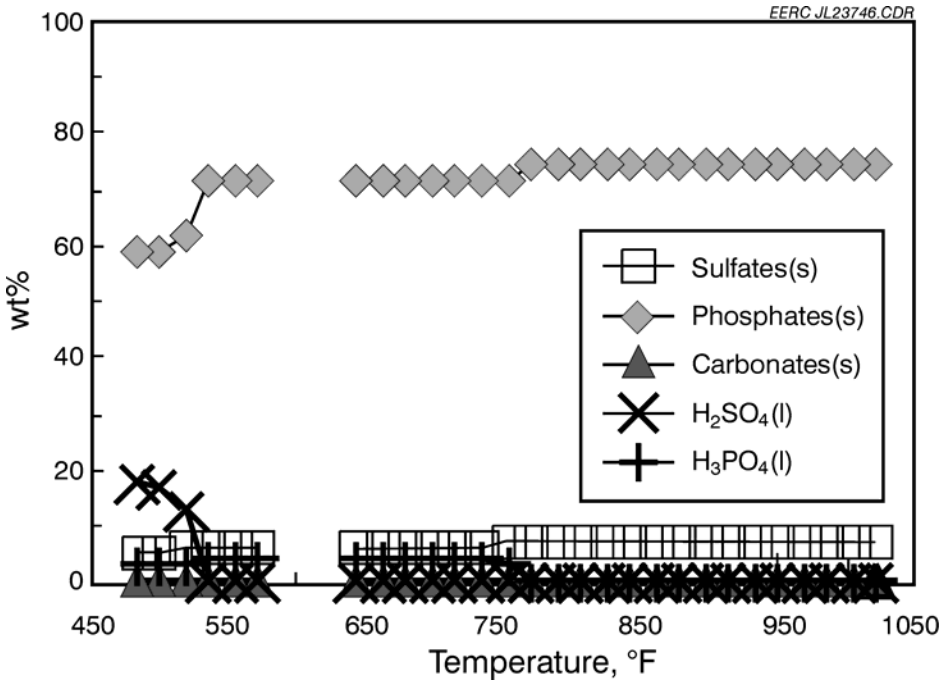

Figure 10. FACT modeling results for Beulah with 300 ppm ammonia and 1000 ppm P_2O_5.

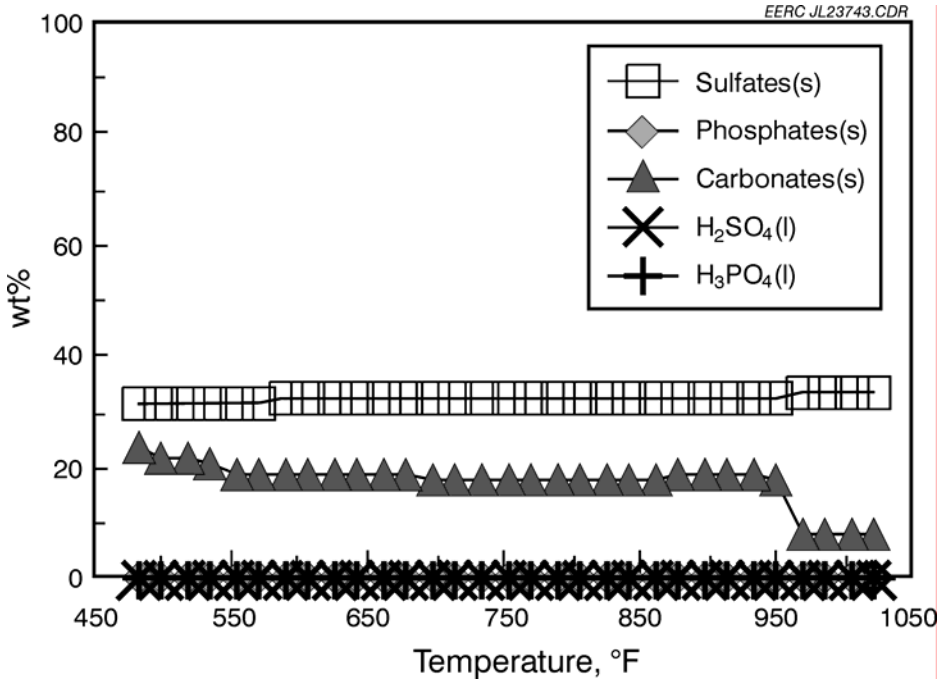

Figure 11. FACT modeling results for Nanticoke PRB with 100 ppm ammonia and 1 ppm P_2O_5.

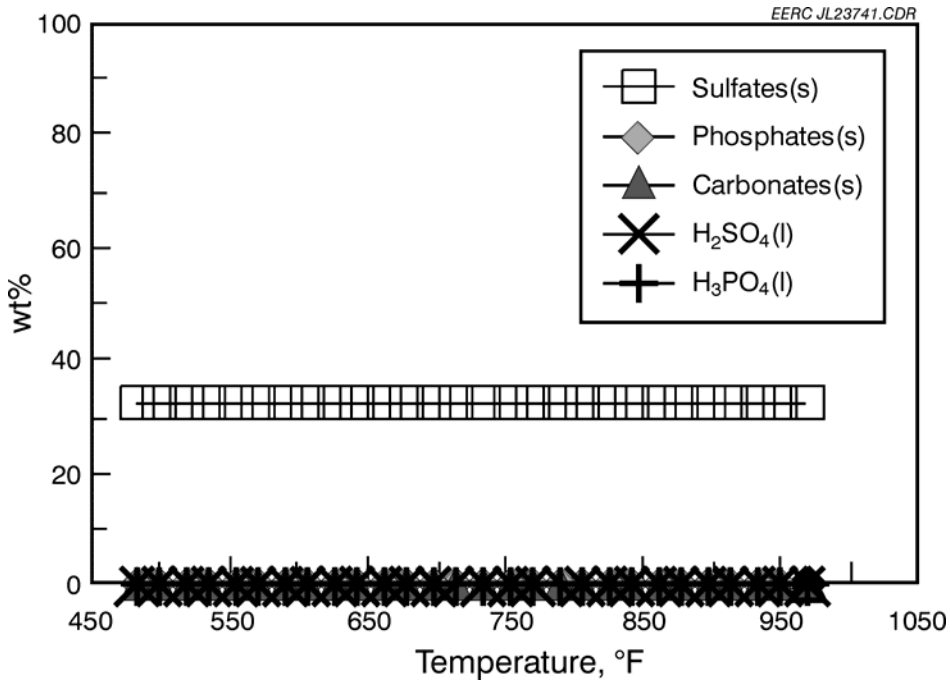

Figure 12. FACT modeling results for Nanticoke PRB–LSUS blend with 100 ppm ammonia and 1 ppm P_2O_5.

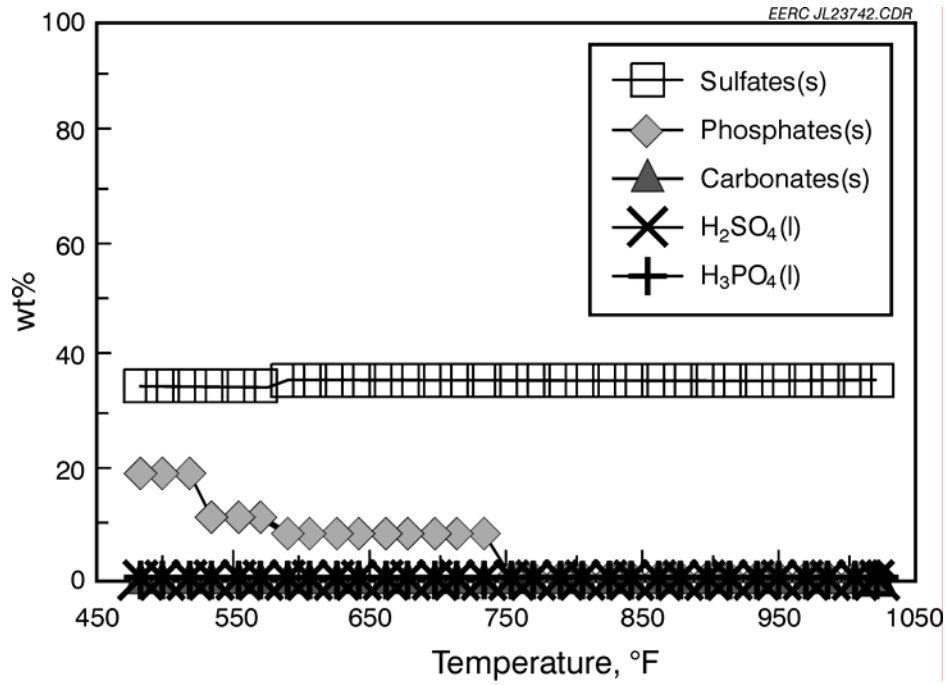

Figure 13. FACT modeling results for Beulah with 100 ppm ammonia and 1 ppm P_2O_5.

Characterization of Reaction Products from Bench-Scale Tests

The reaction products from three of the bench-scale tests were analyzed with SEM to validate the FACT modeling and to determine that the material gained during the tests was indeed a sulfate. Figures 14–16 are SEM micrographs of the fly ash from the Nanticoke PRB, Nanticoke PRB–LSUS blend, and the Beulah lignite. Corresponding Tables 8–10 contain the chemical analysis of several fly ash particles. Sulfur is present in almost all analyses and increases along with calcium. This indicates that most of the sulfur is present as calcium sulfate. These results are also consistent with the FACT modeling predictions. One exception may be that phosphates were not present in large quantities.

Task 3 – Design and Construction of the SCR Slipstream Test Chamber

The SCR slipstream system consists of two primary components: the control room and the SCR reactor. The reactor section consists of a catalyst section, an NH_3 injection system, and sampling ports for NO_x at the inlet and exit of the catalyst section. The control room houses a computer system that logs data and controls the gas flow rates, temperatures, pressure drop across the catalyst, and sootblowing cycles. The computer was programmed to maintain constant temperature of the catalyst, gas flow rates, sootblowing cycles, and NH_3 injection. The computer is equipped with a modem that allowed for downloading of data and modification of the operation of the reactor from a remote computer located at the EERC.

A schematic diagram of the SCR slipstream system is shown in Figure 17. Flue gas is isokinetically extracted from the convective pass of the boiler upstream of the air heater. The temperature is typically about 790°F. The flue gases pass through a 4-inch pipe equipped with sampling, thermocouple, and pressure ports. NH_3 is injected into the piping upstream of the reactor section. The reactor consists of a steel housing that is approximately 8.5 inches square and 8 feet long. The reactor section illustrated in Figure 18 has three components, including a flow straightener, a pulse section or sootblower, and a catalyst test section. A metal honeycomb is used as a flow straightener upstream of the catalyst section and is about 6 inches long. A purge section was installed ahead of the catalyst test section to remove accumulated dust and deposits. The catalyst test section is located downstream of the purge section. The entire catalyst section is insulated and equipped with strip heaters for temperature control. The catalyst test section is 1 m (3.28 ft) in length and houses three catalyst sections. Thermocouple and pressure taps are located in the purge sections for measurements before and after each section.

The induced-draft fan is used to extract approximately 5.6 scmm (200 scfm) of flue gas from the convective pass of the utility boiler to achieve an approach velocity of 5.2 m/s (17.0 ft/s). The total gas flow through the reactor represents a thermal load of approximately 300 kW.

The range of operating conditions for the reactor is listed below:

- Gas temperature: ~371°–426°C (700°–800°F)
- Gas flow rate: 11.3–14.2 acmm (400–500 acfm)
- Approach velocity range: 5.0–5.5 m/sec (16.4–18 ft/s)

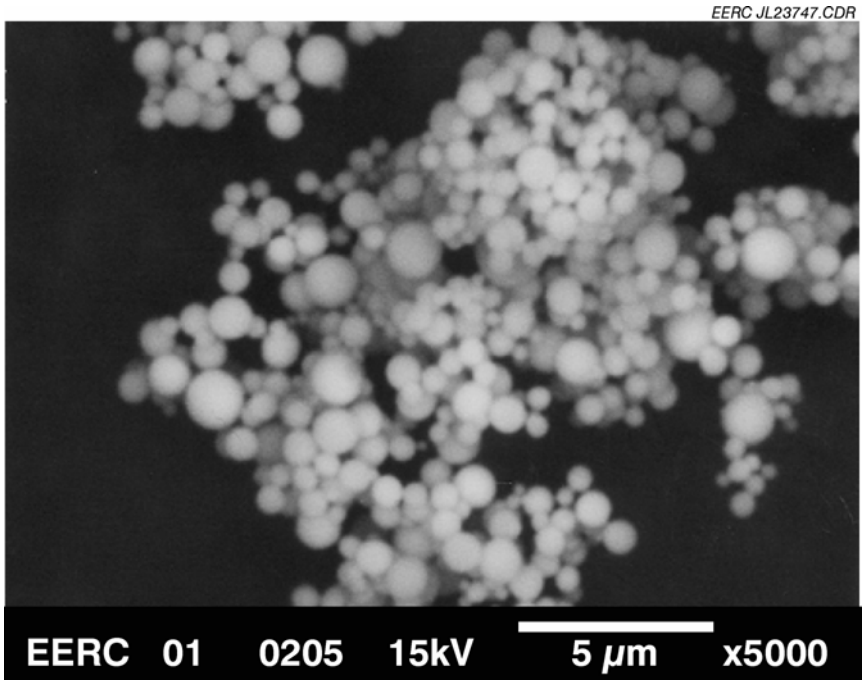

Figure 14. SEM micrograph of reaction products from Nanticoke PRB.

Table 8. SEM/Energy-Dispersive Spectroscopy (EDS) Analysis Results from Nanticoke PRB at 800°F

Element	Percent	Percent
Na	0.50	0.00
Mg	5.60	5.00
Al	9.22	11.30
Si	9.00	8.30
P	1.80	1.30
S	0.70	2.10
Cl	0.00	0.00
K	0.30	0.00
Ca	32.40	31.00
Ti	0.00	1.40
Cr	0.00	0.00
Fe	11.60	7.70
Ba	1.50	1.10
O	27.00	30.60

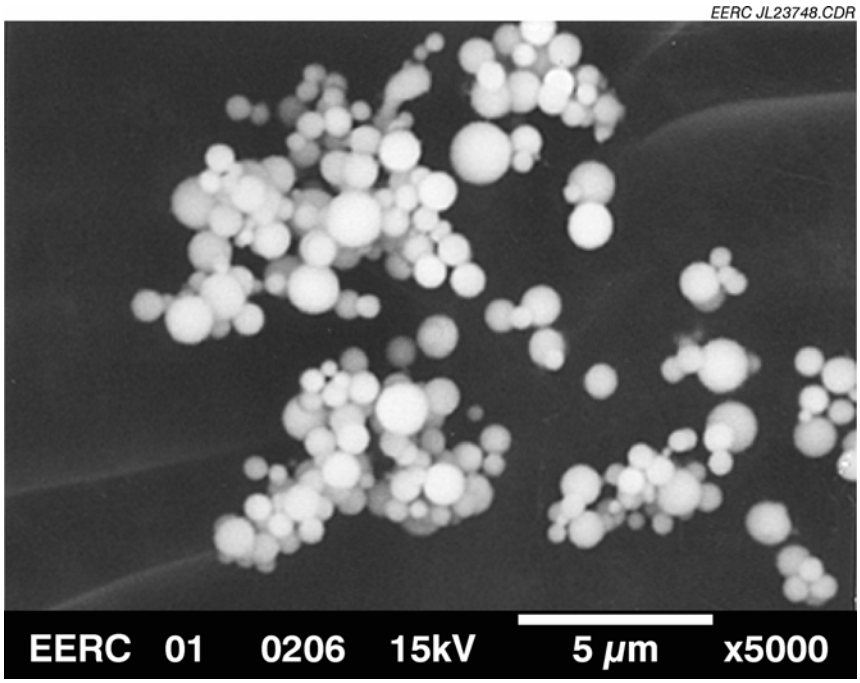

Figure 15. SEM micrograph of reaction products from Nanticoke PRB–LSUS blend.

Table 9. SEM/EDS Analysis Results from Nanticoke PRB–LSUS blend at 800°F

Element	Percent	Percent
Na	0.40	0.50
Mg	2.10	3.10
Al	15.90	12.60
Si	14.50	21.80
P	2.00	4.00
S	1.00	0.00
Cl	0.10	0.00
K	1.70	1.00
Ca	20.00	10.60
Ti	0.90	3.00
Cr	0.00	0.00
Fe	4.90	5.60
Ba	0.00	1.00
O	36.40	36.50

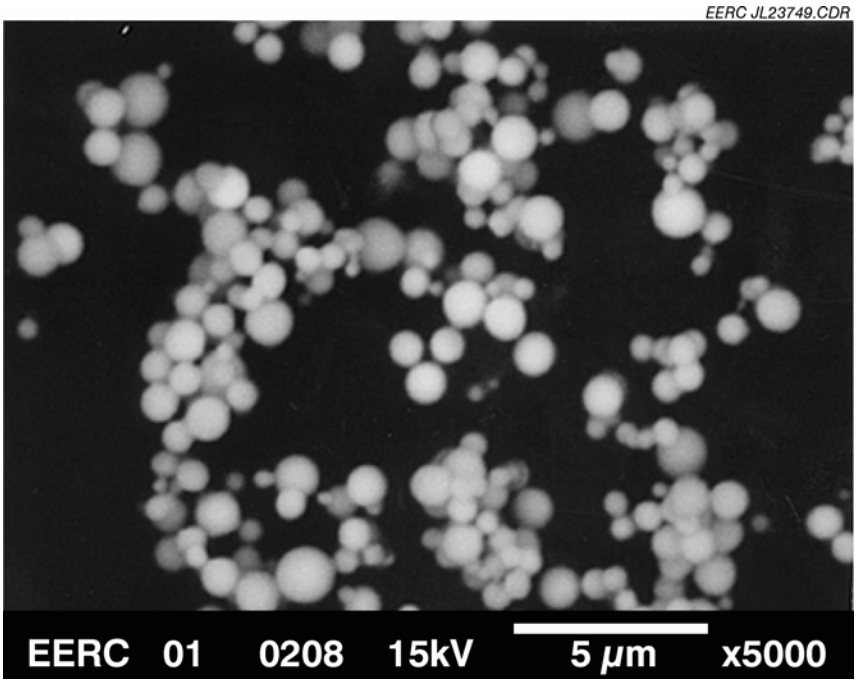

Figure 16. SEM micrograph of reaction products from Beulah lignite.

Table 10. SEM/EDS Analysis Results from Beulah Lignite at 800°F

Element	Percent	Percent
Na	1.60	1.00
Mg	4.00	5.30
Al	7.10	9.00
Si	22.70	18.10
P	0.00	0.00
S	1.60	2.80
Cl	0.00	0.00
K	1.40	0.50
Ca	17.10	25.00
Ti	0.00	1.50
Cr	0.10	0.00
Fe	5.40	4.00
Ba	5.90	4.60
O	33.00	28.00

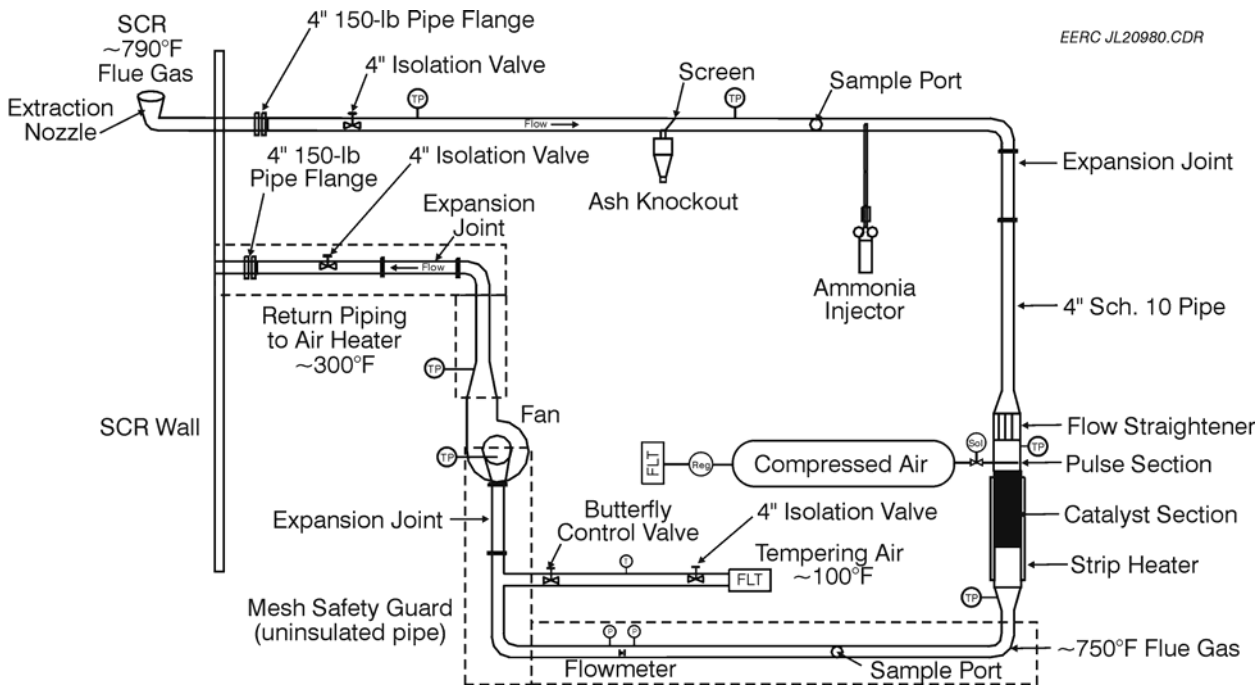

Figure 17. Conceptual schematic of the SCR reactor slipstream field test unit.

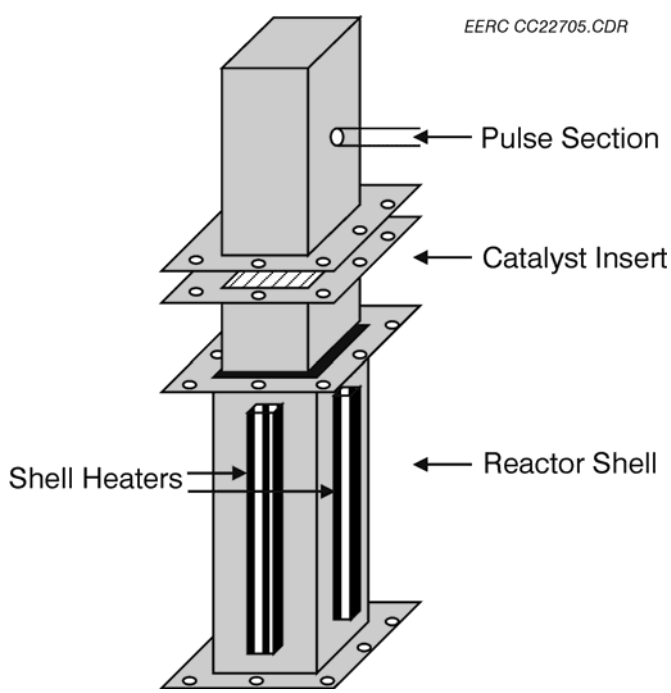

Figure 18. SCR catalyst section.

- NH_3 injection rate: 0.5:1 with NO_x level
- Tempering air for fan: ~1.4–5.7 scmm (50–200 scfm)
- Catalyst dP: 0.5–1.0 inches water column
- Fan sized for up to 30 inches water column

For catalyst inspection or replacement, the catalyst section can be unbolted and slid out from the reactor (support brackets hold the remaining reactor pieces in place). Once a catalyst reactor section is removed, the top catalyst holder can be removed, and the section(s) of interest removed by pushing it up from the bottom and out the top. A new section is then inserted from the top to replace the piece removed.

Task 4 – SCR Test Chamber Installation and Data Collection at Utility Host Sites

The catalyst installed at the Baldwin and Coyote Stations was the Haldor Topsoe catalyst. Topsoe's DNX-series of catalysts comprises SCR DENOX catalysts tailored to suit a comprehensive range of process requirements. DNX-series catalysts are based on a corrugated, fiber-reinforced TiO_2 carrier impregnated with the active components V_2O_5 and tungsten trioxide (WO_3). The catalyst is shaped to a monolithic structure with a large number of parallel channels. The unique catalyst design provides a highly porous structure with a large surface area and an ensuing large number of active sites. Figure 19 is an image of the Haldor Topsoe SCR catalyst. The pitch of the catalyst was approximately 6 mm.

Figure 19. Haldor Topsoe SCR catalyst showing the gas flow passages.

The catalyst installed at the Columbia Station was a Babcock Hitachi plate-type catalyst. This catalyst is a TiO_2-based plate catalyst, developed and manufactured by Hitachi. Figure 20 shows the design of the catalyst. The pitch of the catalyst was approximately 10 mm.

Upon installation at each utility boiler unit, flue gas temperature, composition, and velocity measurements were obtained using portable equipment. Shakedown testing of the unit was conducted to ensure that all components were operating properly and that data were being logged and could be retrieved. After installation and shakedown were completed, the reactor was operated in a computer-controlled, automated mode and monitored on a daily basis to ensure proper operation and data quality. During operation of the SCR slipstream system, catalyst temperature, sootblowing frequency, and pressure drop across the catalyst were monitored and logged. Samples of the exposed SCR catalyst and associated deposits were obtained after exposure to flue gas and particulate for 2, 4, and 6 months. The samples of the catalyst were analyzed to determine the components that were bonding and filling pores, resulting in decreased reactivity.

The characteristics of ash that accumulated on the catalyst were examined using SEM–x-ray microanalysis and XRD (18). Correlations between the physical and chemical characteristics of any ash deposits on the SCR test section and entrained-ash sample collected at the chamber inlet and the coal inorganic composition were made to discern mechanisms of SCR blinding. Entrained ash was collected at Columbia Station only and characterized as to composition and size.

Figure 20. Babcock Hitachi SCR catalyst showing the gas flow passages.

Baldwin Station Data

The data presented in the following section represent a small portion of the operational data collected. The remainder of the data is available upon request. The reactor was installed at the Baldwin Station and operated for a 6-month time period on the Haldor Topsoe catalyst. The information obtained from testing included pressure drop, sootblowing cycles, and reactor temperatures. Table 11 summarizes the operating conditions of the reactors during the testing periods at all plants. Figures 21–23 show the pressure drop across the catalyst test periods from 0 to 2 months, 2 to 4 months, and 4 to 6 months, respectively. During the first 2 months of operation, the pressure shown in Figure 21 was about 0.5 inches of water; at the end of 2 months, the pressure drop was about 0.8 inches of water, indicating plugging had occurred. The air was pulsed a minimum of every 8 hours in an attempt to maintain cleanliness. The reactor was monitored on a daily basis, and adjustments in pulsing cycles were made in order to minimize deposit accumulation. However, for the first 2 months, the pressure drop steadily increased. During several periods when the unit was taken off-line, the temperature of the catalyst was maintained. At 2-month intervals, a section of catalyst was removed and replaced with a new one.

For Months 2 through 4, the pressure drop was highly variable initially but was about 0.8 inches of water. From Months 4 through 6, the pressure drop was maintained between 0.6 and 0.8 inches of water. This is due to the installation of a fresh catalyst section and leaving two-thirds of the catalysts in place that were partially plugged. The gas velocity in the single section of new, clean catalyst was high because of channeling, and the result of the high gas flow was less deposition and accumulation. Gas velocity has a significant impact on the potential for deposits to form. However, at high gas velocity, low NO_x conversion is likely.

Columbia Station Data

The reactor was installed at the Columbia Station and operated for a 6-month period of time for the Babcock Hitachi catalyst. The information obtained from the testing included pressure drop information, sootblowing cycles, and reactor temperature. Table 11 shows the reactor temperature, air-pulsing cycles, and airflow rates. Figures 24–26 show the test periods from 0 to 2 months, 2 to 4 months, and 4 to 6 months, respectively. The pressure drop across the SCR upon installation was about 0.4 inches of water and increased to an average of about 0.5 inches of water, but ranged from less than 0.4 to greater than 0.8 inches of water. Figure 25

Table 11. Selected Operating Conditions of the SCR Catalysts

Plant Name	Average SCR Inlet Temp., °F	Average SCR Outlet Temp., °F	Air Pulse Frequency	Flue Gas Flow Rate, acfm
Baldwin	645	549	Once a day and on demand	393
Columbia	672	662	Once a day and on demand	385
Coyote	675	667	Once a day and on demand	385

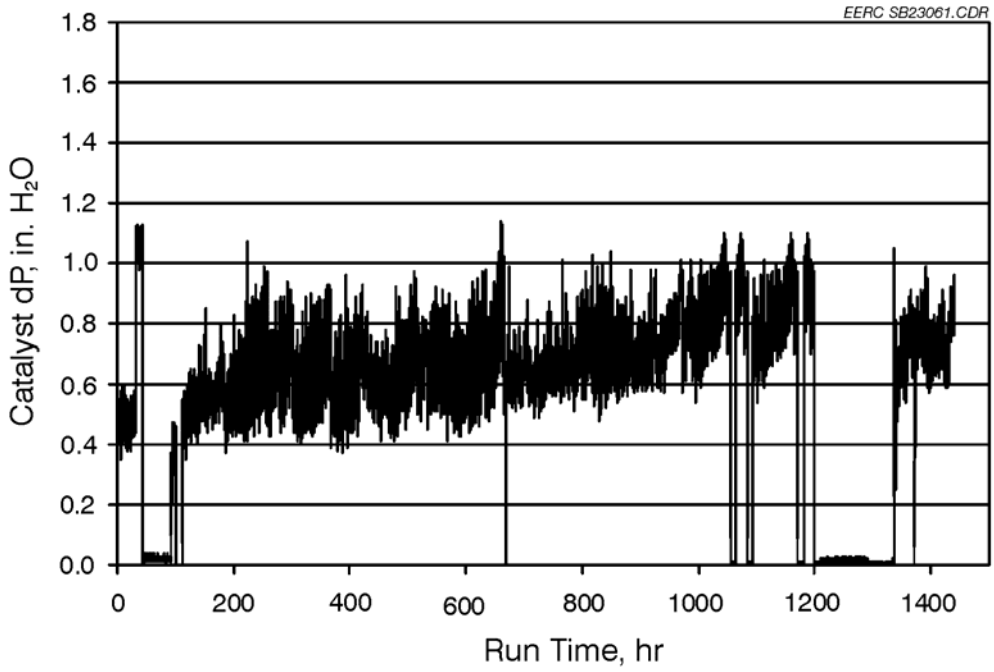

Figure 21. Catalyst pressure drop at Baldwin Station at 0 to 2 months of operation.

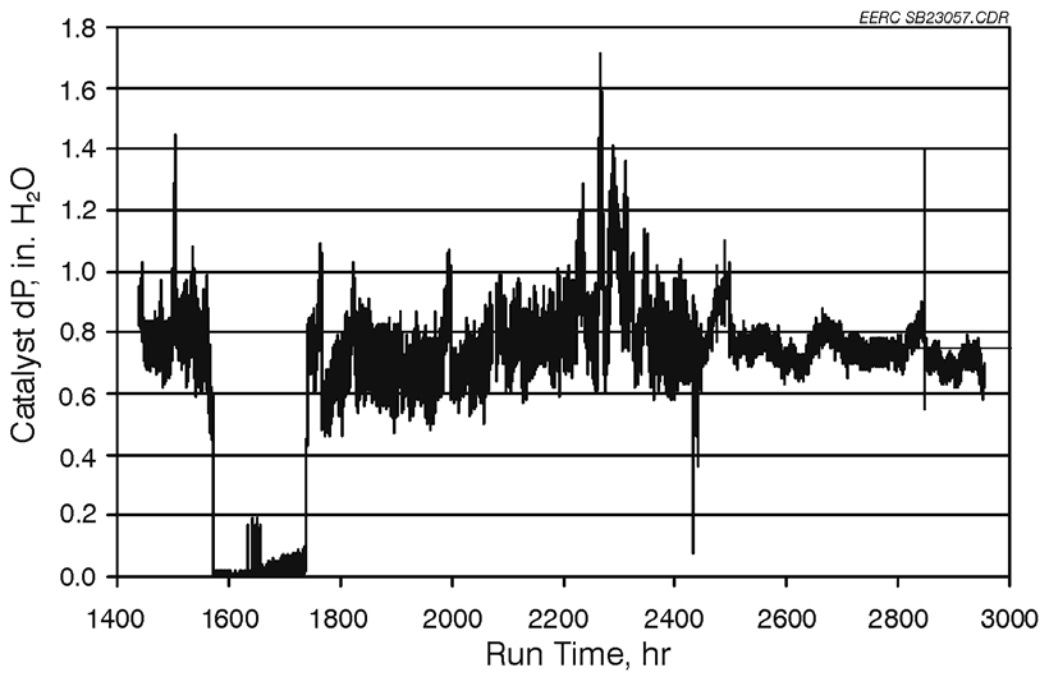

Figure 22. Catalyst pressure drop at Baldwin Station at 2 to 4 months of operation.

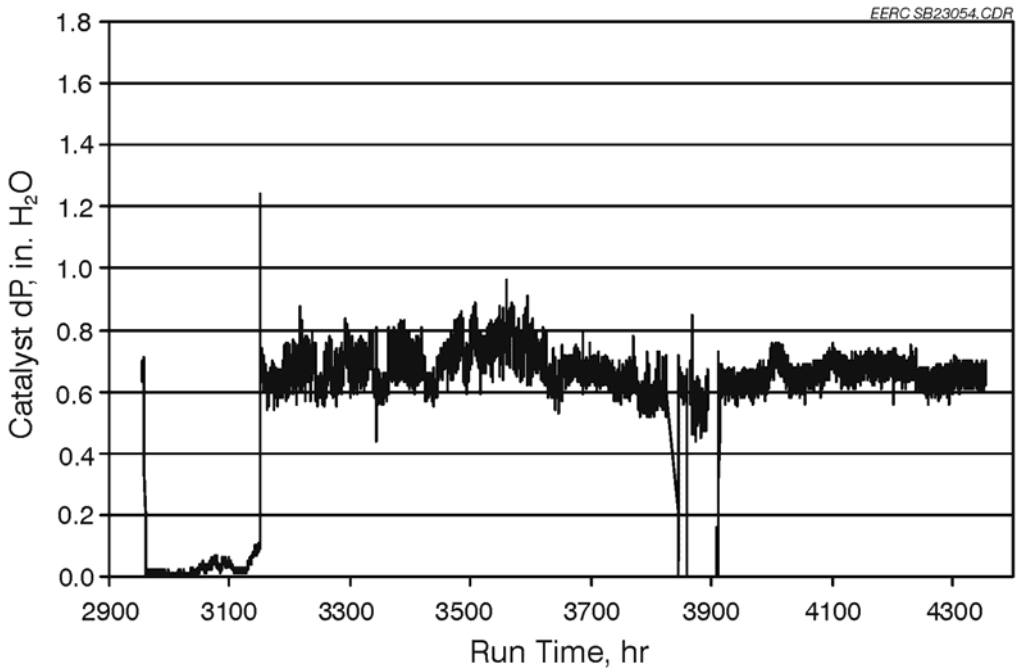

Figure 23. Catalyst pressure drop at Baldwin Station at 4 to 6 months of operation.

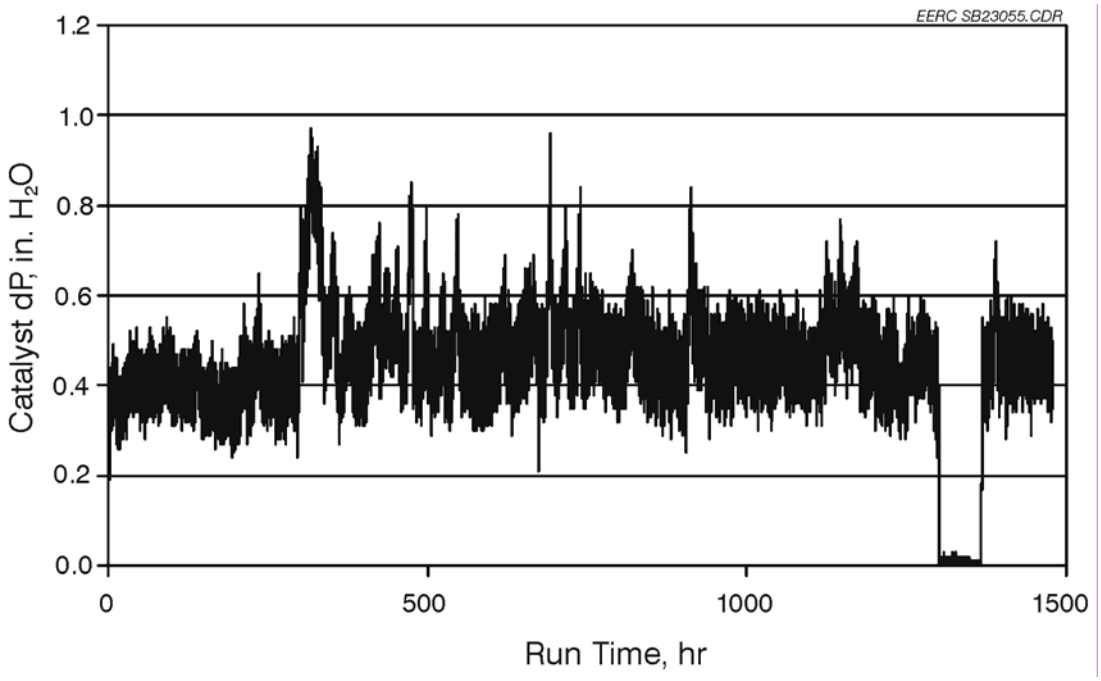

Figure 24. Catalyst pressure drop at Columbia Station at 0 to 2 months of operation.

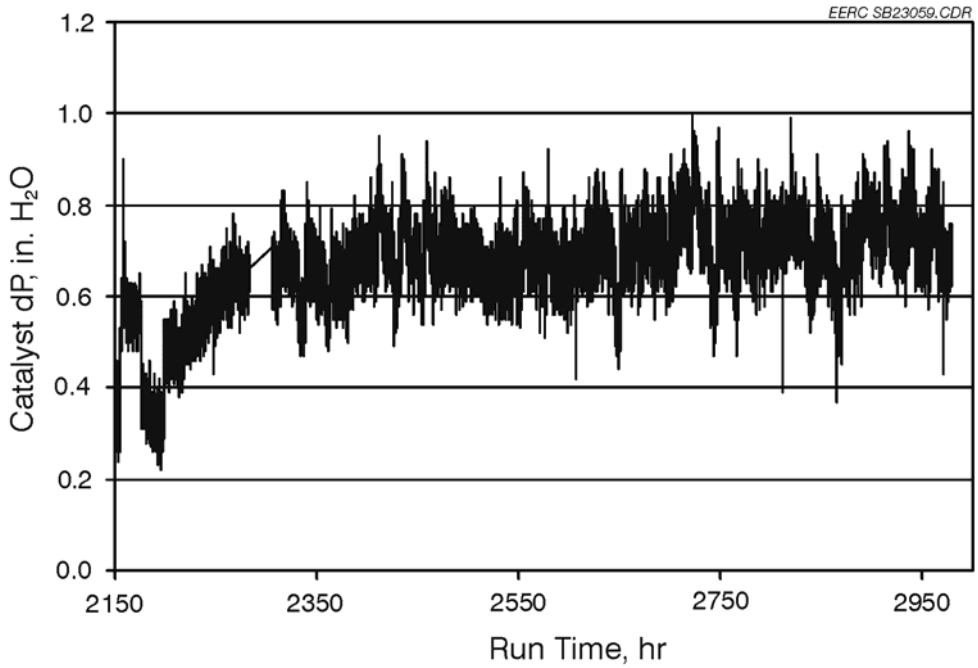

Figure 25. Catalyst pressure drop at Columbia Station at 2 to 4 months of operation.

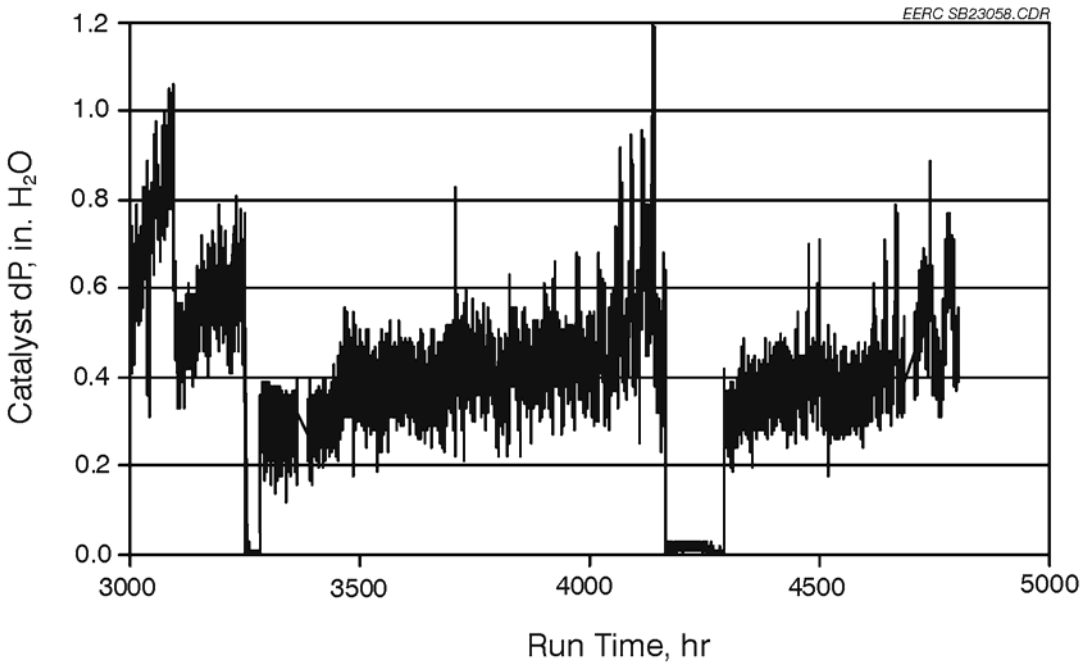

Figure 26. Catalyst pressure drop at Columbia Station at 4 to 6 months of operation.

shows the pressure drop for Months 2–4. The pressure drop increased from about 0.5–0.7 inches of water because of accumulation of ash. Figure 26 shows a rapid increase in pressure drop across the catalyst at about 3000 hours of operation, and aggressive pulsing brought it down to 0.4 inches of water until the catalyst section was changed out at about 3200 hours. After the reactor was cleaned and one catalyst section was replaced, the pressure drop was about 0.3 but increased to over 0.6 inches of water up to about 4100 hours. There was an outage at the plant, and aggressive pulsing of the reactor was conducted; the pressure drop was brought back down to 0.3 but rapidly increased to over 0.5 inches of water within 500 hours.

Coyote Station Data

The same reactor that was installed at the Baldwin Station was moved and installed at the Coyote Station. In addition, the same Haldor Topsoe catalyst formulation was used in the reactor. The cleaning cycles, temperatures, and gas flow rates are listed in Table 11. The reactor was operated for 6 months. Figures 27–29 show the test periods from 0 to 2 months, 2 to 4 months, and 4 to 6 months, respectively. The pressure drop across the catalyst upon installation was about 0.4 inches of water. After only 750 hours, the pressure drop was 1.5 inches of water, indicating significant plugging and blinding. Aggressive air pulsing was conducted, with little success in removing the deposits. The pressure drop for the catalyst was over two times greater than the pressure drop observed for the Baldwin Station utilizing the same reactor and the same catalyst. At about 1700 hours, the reactor was cleaned, and a section of catalyst was removed for characterization. The pressure drop after cleaning was 0.8–1.0 inches of water. The pressure drop did not increase as rapidly because of the higher velocities through the clean section of the catalyst. Figure 29 shows the pressure drop for 4–6 months of operation. The pressure drop

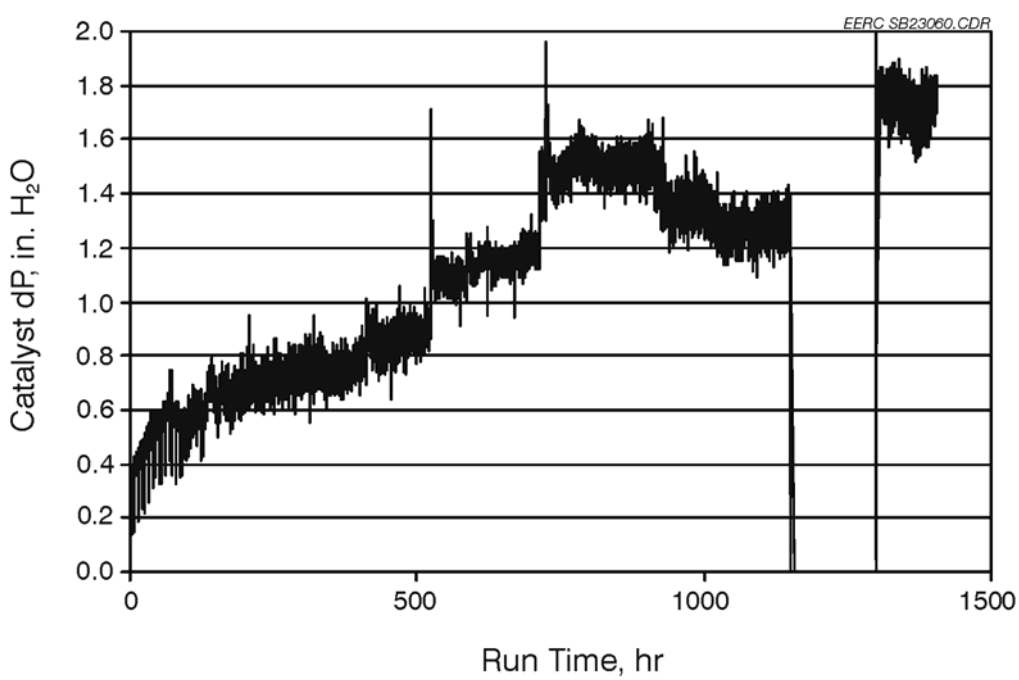

Figure 27. Catalyst pressure drop at Coyote Station at 0 to 2 months of operation.

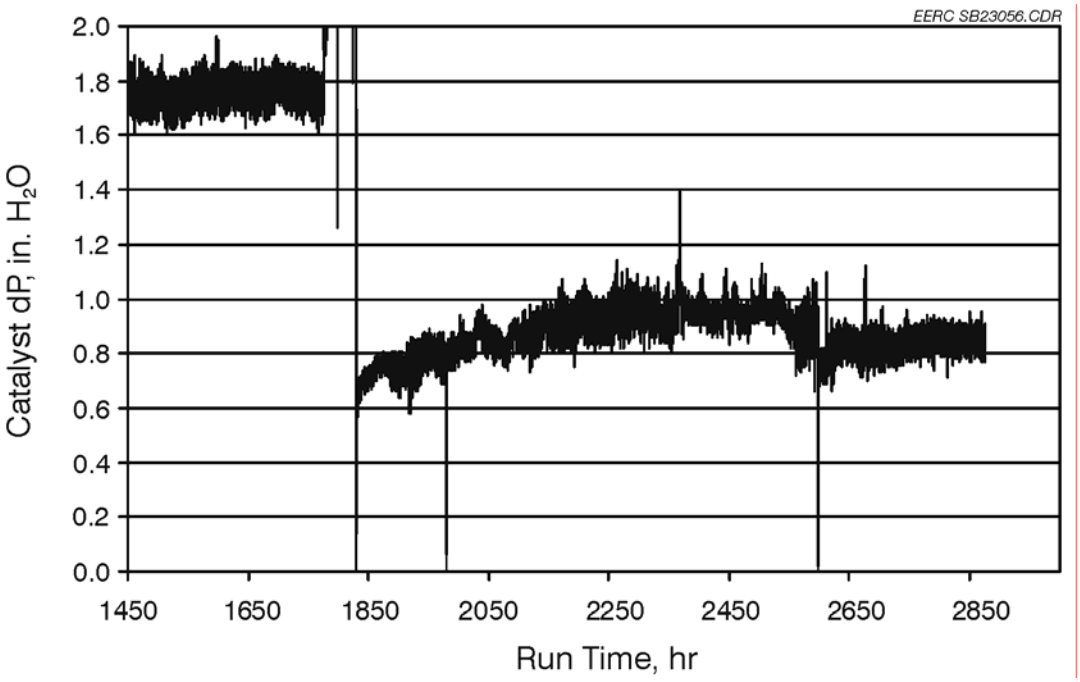

Figure 28. Catalyst pressure drop at Coyote Station at 2 to 4 months of operation.

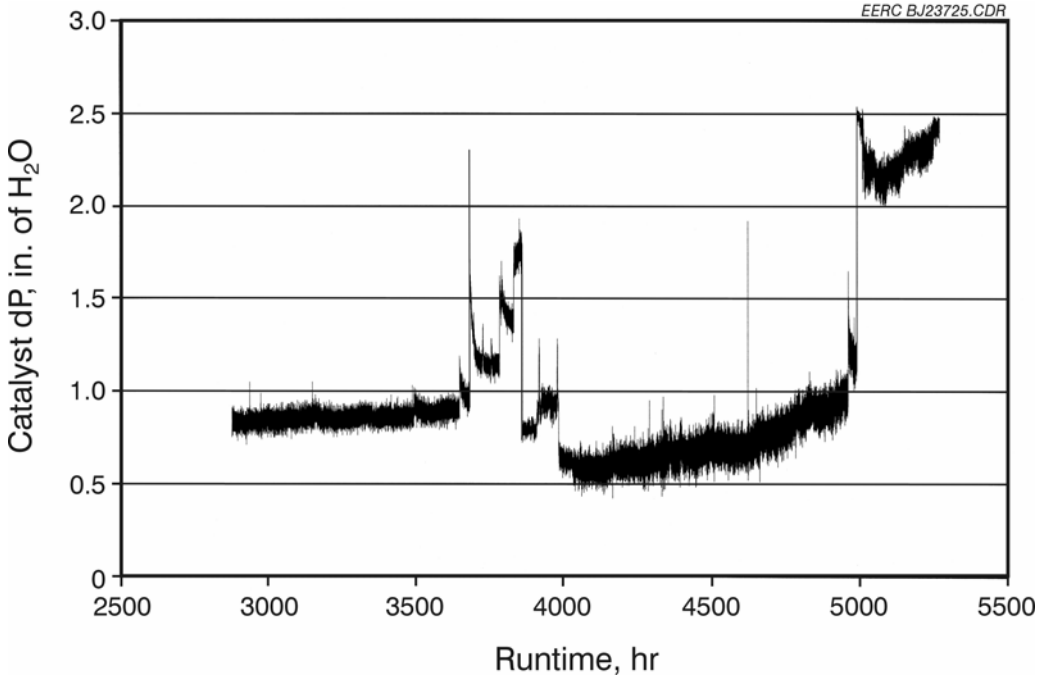

Figure 29. Catalyst pressure drop at Coyote Station at 4 to 6 months of operation.

during the last 2 months of testing was highly variable and at times reached values over 2 inches of water.

Visual Observations and Chemical Analysis

The tops of the catalysts were photographed during inspection and sampling of the catalyst sections. Figure 30 shows the ash materials that accumulated on the catalyst inlet after 2 months of operation. The most significant accumulation was noted for the Coyote Station, followed by Columbia and Baldwin. The Coyote Station had some larger pieces of ash deposit material on the surface as well as plugging of the catalyst passages. The Baldwin Station showed some obvious deposition along the walls of the reactor and some accumulation on the inlet sections. The Columbia Station showed more significant accumulation and plugging than the Baldwin Station. After 4 months, the tops of the catalysts were photographed during inspection and sampling of the catalyst sections, as shown in Figure 31. The most significant accumulation was noted for the Coyote Station and some accumulation for the Baldwin Station.

The ash materials that collected on the catalyst surfaces and pores were characterized by SEM and x-ray microanalysis, and in selected cases, XRD was used to determine the crystalline phases present. The catalysts were sampled after 2, 4, and 6 months. The sections were sampled, and approximately 2.5-cm squares were mounted for SEM analysis on double-stick tape and in epoxy resin. The double-stick tape samples allowed for characterization of the external morphology of the particles and catalyst surface. The samples mounted in resin were cross-sectioned and polished, which allowed for more detailed and quantitative analysis of the bonding materials and materials that accumulated in the pores of the catalyst. The data presented in the following section represent a small portion of the data collected by SEM analysis. The remainder of the data is available upon request.

Baldwin Station Deposits

Samples of catalyst were removed from the Baldwin Station after exposure to flue gas and particulate after 2, 4, and 6 months. Figure 32 shows the characteristics of the ash deposit material on the SCR catalyst after 2 months of exposure. This is a polished cross section of a deposit on the surface of the catalyst. Figure 32a shows particles on the surface of the catalyst that range in size from <1 to 15 µm. The larger particles range from oxides of solely silicon and iron to complex mixtures rich in aluminum and calcium; aluminum, silicon, and calcium; aluminum, calcium, and iron; and sodium, calcium, aluminum, and silicon. Chemical analysis of selected particles is summarized in Table 12. The samples of ash mounted on double-stick tape allow for the characterization of the external surfaces of the particles. The surface of a typical particle that is accumulating on the surface of the catalyst is shown in Figure 32b. The blebs on the surface are composed of calcium and sulfur, with some iron and minor amounts of sodium and potassium. Figure 32c shows a cross section of the deposited particles showing calcium- and aluminum-rich particles bonded together with a calcium- and sulfur-rich phase. This phase is in the form of calcium sulfate based on XRD analysis conducted on the deposited ash samples.

The 4-month sample from the Baldwin Station showed more extensive sulfation of the alkaline-earth elements present in the deposits. Figure 33 shows the images of a polished cross

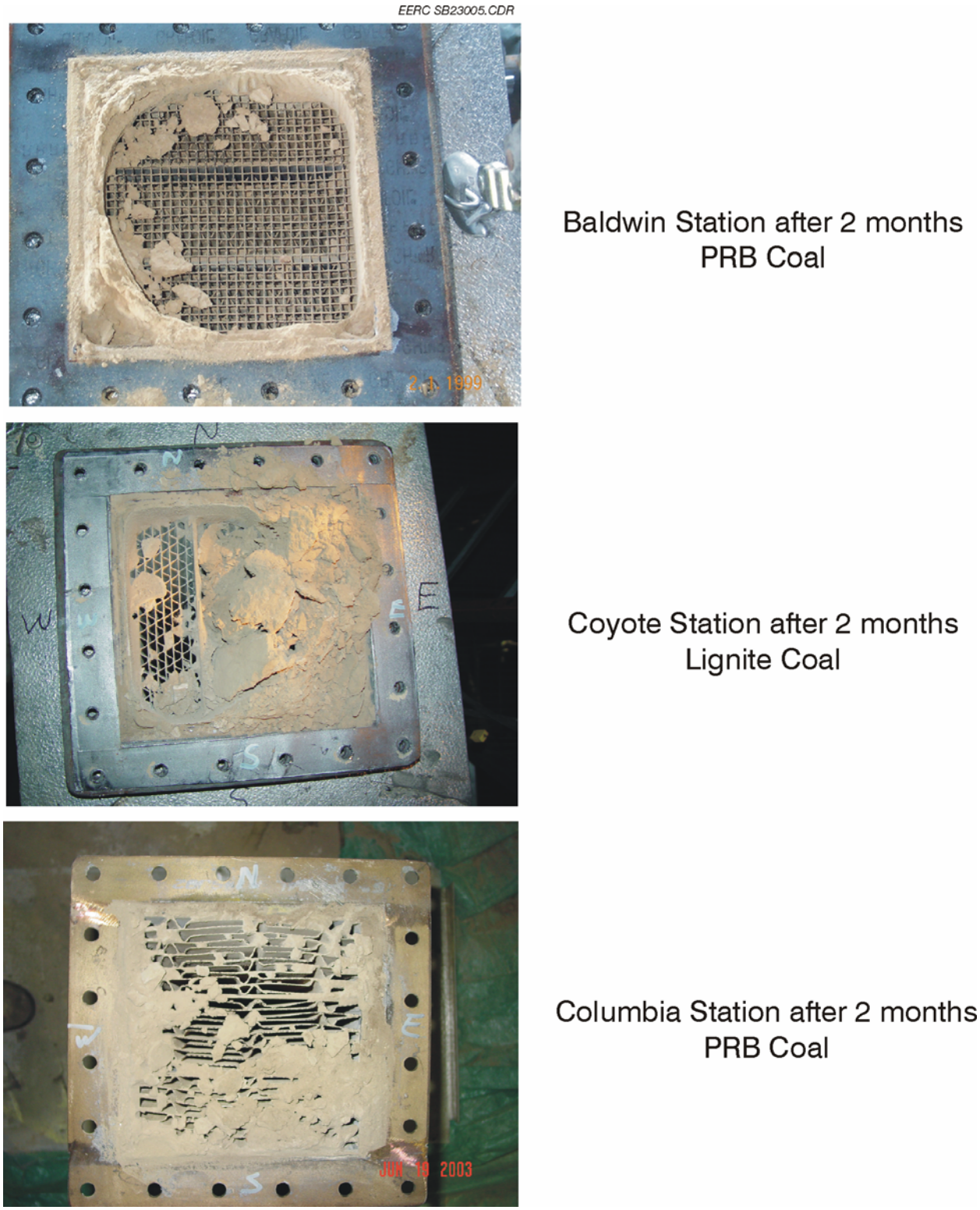

Figure 30. Pictures of catalyst inlet after about 2 months of testing at each plant.

Baldwin Station after 4 months
PRB Coal

Coyote Station after 4 months
Lignite Coal

Figure 31. Pictures of catalyst inlet after about 4 months of exposure to flue gas and particulate.

section of an ash deposit on the surface of the catalyst. The deposit formed both on the surface of the catalyst and within the catalyst pores, as shown in Figure 33a. Figure 33b shows a higher-magnification view of the deposit on the catalyst surface. The deposit consists of particles of fly ash bonded together by a matrix of calcium- and sulfur-rich material, likely in the form of calcium sulfate. The chemical composition of selected points shown in Table 13 shows high levels of calcium and sulfur. There is much more extensive bonding of the materials with the sulfate matrix as compared to the 2-month sample.

The 6-month sample from the Baldwin Station showed extensive sulfation of the alkaline-earth elements present in the deposits. Figures 34a and 34b show regions of the catalyst where all the pores were blocked and a minimal amount of deposit on the surface of the catalyst. Figure 34c shows a higher-magnification view of the deposit that is filling the catalyst pore. The deposit consists of particles of fly ash bonded together by a matrix of calcium- and sulfur-rich material, likely in the form of calcium sulfate. The chemical compositions of selected points that

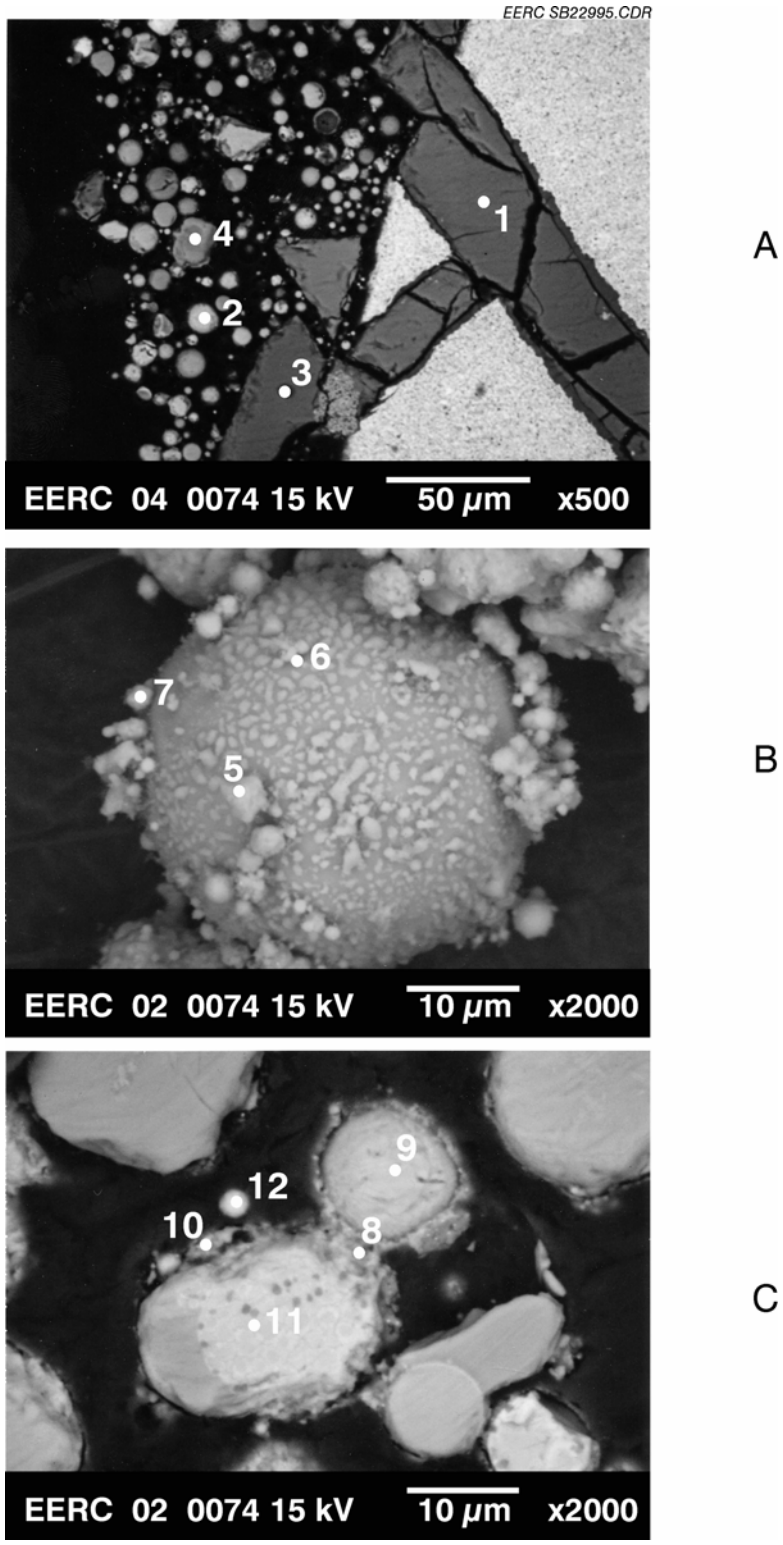

Figure 32. SEM images of ash collected on catalyst surface at the Baldwin Station after 2 months of exposure: A) low-magnification image of ash deposit on catalyst surface, B) high-magnification image of coated ash particle, and C) high-magnification image of polished cross section showing coatings on particles.

Table 12. Chemical Composition of Selected Points and Areas in Figure 32

	Element, wt%					
	Point 1	Point 2	Point 3	Point 4	Point 5	Point 6
Oxide						
Na_2O	0.2	0.0	0.2	2.3	2.5	3.0
MgO	0.0	6.3	0.0	3.1	3.0	1.3
Al_2O_3	3.6	17.9	6.9	29.6	8.4	5.5
SiO_2	92.1	5.9	86.5	39.9	3.4	53.2
P_2O_5	0.1	0.4	0.0	0.0	1.8	0.0
SO_3	3.3	0.4	5.2	0.1	51.8	18.1
K_2O	0.0	0.0	0.0	0.6	0.4	0.5
CaO	0.0	49.4	0.1	18.6	16.4	14.6
TiO_2	0.7	4.5	0.4	1.0	0.0	0.0
Fe_2O_3	0.0	14.6	0.7	3.6	12.3	3.8
BaO	0.0	0.6	0.0	1.1	0.0	0.0
Total	100	100	100	100	100	100
	Point 7	Point 8	Point 9	Point 10	Point 11	Point 12
Oxide						
Na_2O	3.6	0.7	0.6	1.6	0.4	0.9
MgO	1.6	2.5	4.5	3.0	3.6	3.5
Al_2O_3	4.4	5.4	22.7	12.2	21.2	14.2
SiO_2	15.7	3.4	16.1	1.0	8.1	2.3
P_2O_5	1.5	0.3	0.5	2.3	0.0	4.6
SO_3	52.4	53.0	0.0	46.4	0.0	19.7
K_2O	0.7	0.2	0.0	0.1	0.0	0.0
CaO	13.0	28.8	41.5	27.1	51.1	39.2
TiO_2	0.0	0.0	0.0	0.0	0.0	0.0
Fe_2O_3	7.1	5.7	14.2	6.5	15.6	15.6
BaO	0.0	0.0	0.0	0.0	0.0	0.0
Total	100	100	100	100	100	100

indicate the presence of high levels of calcium and sulfur are listed in Table 14. There is much more extensive bonding of the materials with the sulfate matrix as compared to the 2-month sample. In addition, there are some regions of high levels of calcium, aluminum, and sulfur present. The calcium aluminum materials are likely derived from the calcium aluminum phosphate minerals found in the coal fired at this plant.

Columbia Station Deposits

The 2-month sample from the Columbia Station showed particles adhering to the surface and filling pores in the catalyst, as shown in Figure 35. Figure 35a shows the external morphology of the catalyst surface showing particles trapped in the pores of the catalysts. Chemical compositions of selected points are shown in Table 15. The 2-month sample shows significant evidence of sulfation after only 2 months of exposure. It appears to be more

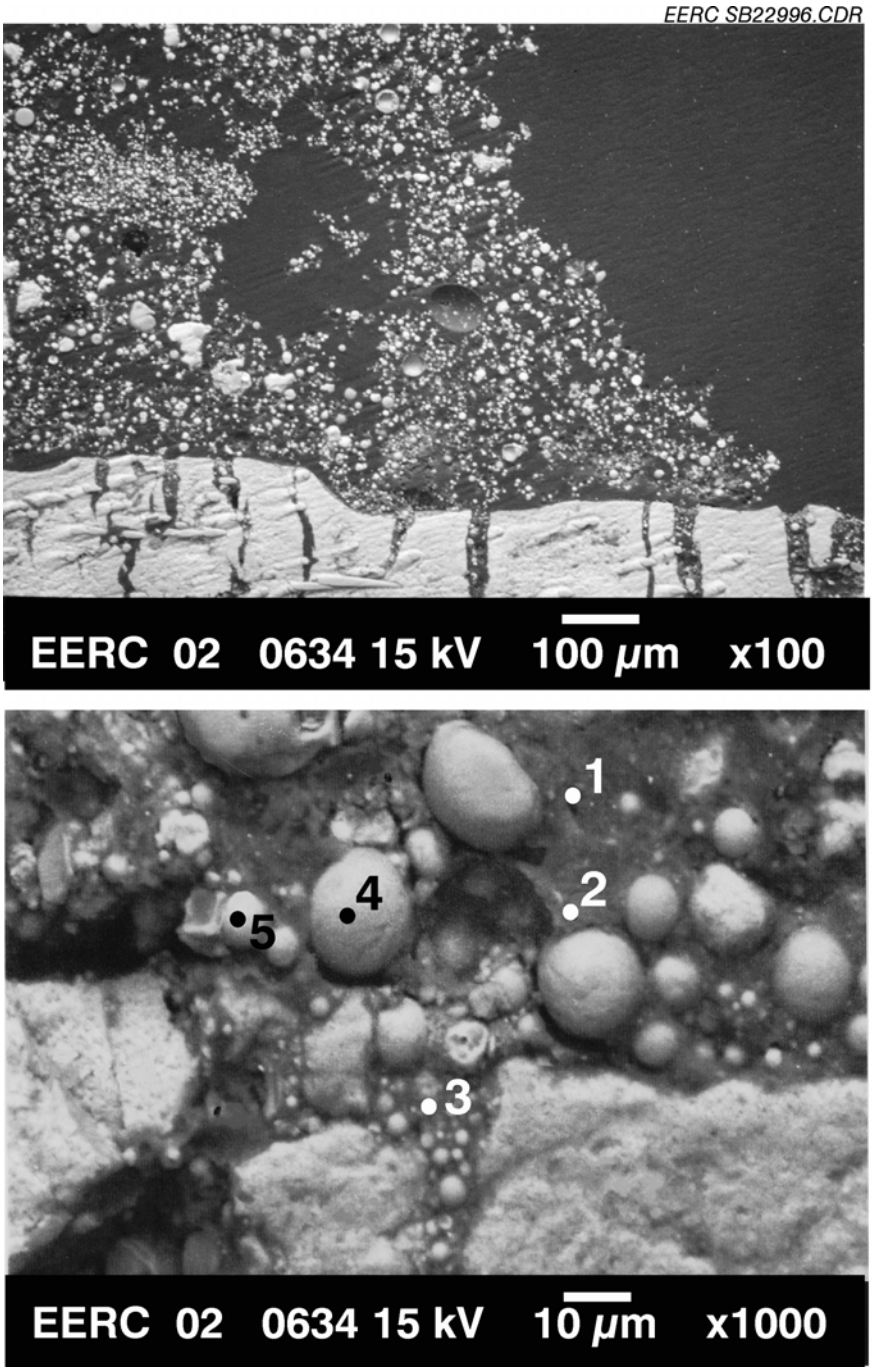

A

B

Figure 33. SEM images of ash collected on catalyst surface at the Baldwin Station after 4 months of exposure: A) low-magnification image of ash deposit on catalyst surface and B) high-magnification image of polished cross section showing particles in a matrix of calcium- and sulfur-rich materials.

Table 13. Chemical Composition of Selected Points and Areas in Figure 33

	Element, wt%				
	Point 1	Point 2	Point 3	Point 4	Point 5
Oxide					
Na_2O	1.7	2.3	0.0	0.3	1.0
MgO	5.9	3.0	1.2	1.8	3.8
Al_2O_3	3.7	2.5	3.3	5.7	6.3
SiO_2	9.7	31.5	13.3	70.0	18.5
P_2O_5	3.1	2.7	0.8	0.0	2.6
SO_3	48.1	31.0	35.8	0.0	32.1
K_2O	0.5	0.7	0.0	1.5	0.0
CaO	22.0	8.8	38.0	13.9	14.7
TiO_2	1.8	10.8	4.1	1.6	15.1
Fe_2O_3	2.1	6.6	3.4	4.2	5.9
BaO	1.4	0.0	0.0	0.9	0.0
Total	100	100	100	100	100

significant than that observed for the Baldwin 2-month sample. Figures 35b and 35c show a higher-magnification view of the deposit that is filling the catalyst pore. The deposit consists of particles of fly ash bonded together by a matrix of calcium- and sulfur-rich material, likely in the form of calcium sulfate.

The 4-month sample from the Columbia Station showed particles adhering to the surface and filling pores in the catalyst, as shown in Figure 36. Figure 36a shows the external morphology of the catalyst surface showing particles trapped in the pores of the catalysts. Chemical compositions of selected points are shown in Table 16. It appears to be more significant than that observed for the Baldwin 2-month sample. Figures 36b and 36c show a higher-magnification view of the deposit that is filling the catalyst pore. The deposit consists of particles of fly ash bonded together by a matrix of calcium- and sulfur-rich material, likely in the form of calcium sulfate.

The 6-month sample from the Columbia Station showed particles adhering to the surface and filling pores in the catalyst, as shown in Figure 37. Figure 37a shows the external morphology of the catalyst surface showing particles trapped in the pores of the catalysts. Chemical compositions of selected points are shown in Table 17. Figures 37b and 37c show a higher-magnification view of the deposit that is filling the catalyst pore. The deposit consists of particles of fly ash bonded together by a matrix of calcium- and sulfur-rich material, likely in the form of calcium sulfate. The 6-month samples show the most extensive degree of sulfation of the Columbia Station samples.

Coyote Station Deposits

The 2-month sample from the Coyote Station showed particles adhering to the surface and filling pores in the catalyst, as shown in Figure 38. Figure 38a shows the external morphology of the catalyst surface showing particles trapped in the pores of the catalysts. Chemical

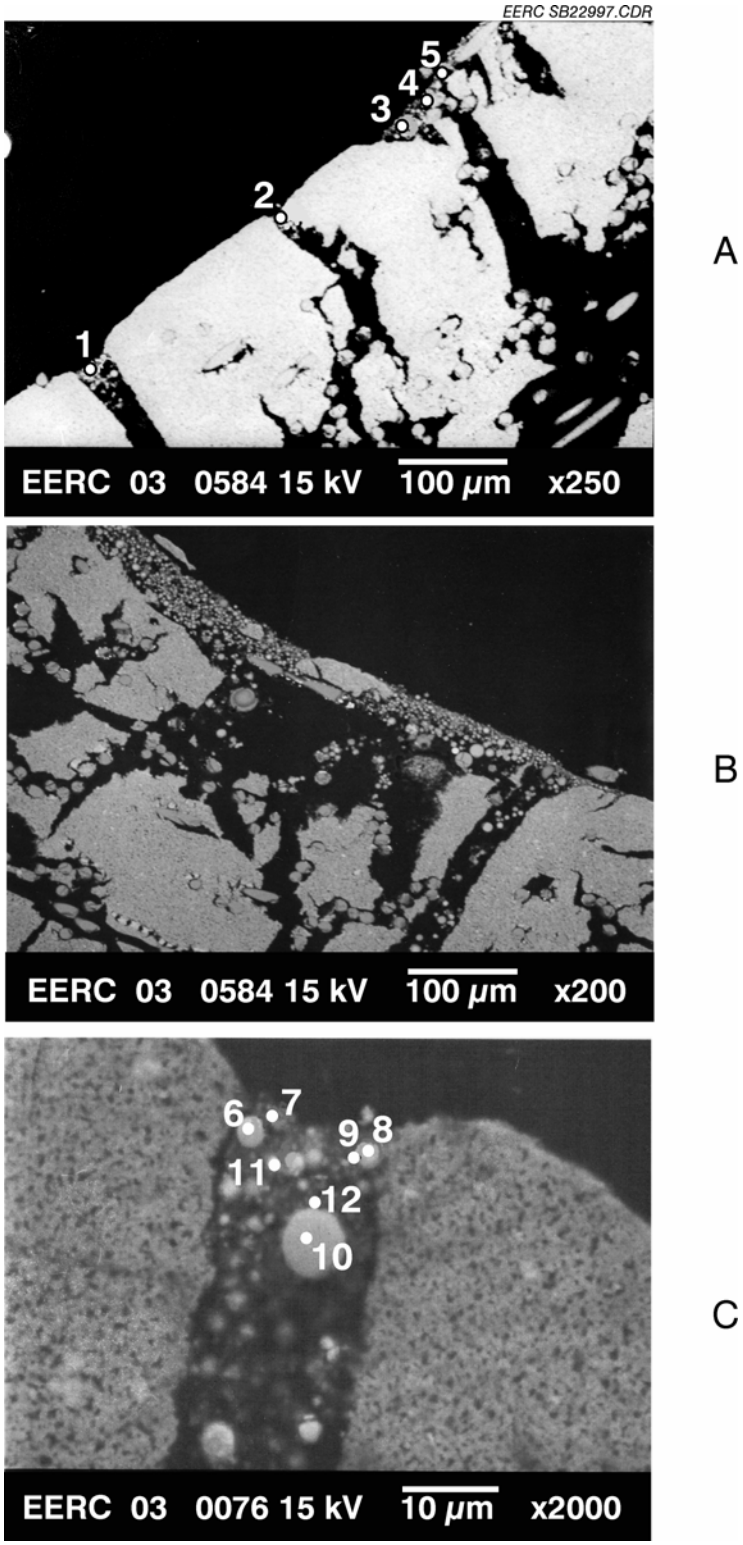

Figure 34. SEM images of ash collected on catalyst surface at the Baldwin Station after 6 months of exposure: A) low-magnification image of ash deposit on catalyst surface, and C) high-magnification image of polished cross section showing particles in a matrix of calcium- and sulfur-rich materials.

Table 14. Chemical Composition of Selected Points and Areas in Figure 34

	Element, wt%					
	Point 1	Point 2	Point 3	Point 4	Point 5	Point 6
Oxide						
Na_2O	0.6	1.0	2.1	0.3	0.5	2.7
MgO	4.3	2.5	6.3	0.7	1.6	7.6
Al_2O_3	14.8	16.0	15.6	15.5	14.7	0.9
SiO_2	3.3	7.8	18.8	57.7	7.7	47.3
P_2O_5	2.3	2.1	0.5	0.6	1.8	0.0
SO_3	30.7	20.4	17.7	0.0	29.0	0.8
K_2O	0.7	0.0	1.0	0.4	0.9	0.9
CaO	28.8	28.7	28.1	22.5	34.9	28.4
TiO_2	2.0	7.2	2.2	0.3	1.3	1.1
Fe_2O_3	11.4	12.9	6.2	0.0	7.6	7.9
BaO	1.1	1.4	1.4	2.0	0.0	2.5
Total	100	100	100	100	100	100
	Point 7	Point 8	Point 9	Point 10	Point 11	Point 12
Oxide						
Na_2O	1.7	0.4	0.5	2.2	1.3	1.7
MgO	4.5	6.4	5.9	5.0	3.4	6.4
Al_2O_3	5.0	2.4	3.0	19.2	10.8	3.8
SiO_2	8.4	18.4	18.5	31.0	17.9	16.7
P_2O_5	1.8	0.9	1.0	0.0	1.7	1.2
SO_3	37.9	1.7	5.3	0.0	22.5	13.9
K_2O	0.4	0.0	0.0	0.9	0.8	0.0
CaO	31.4	52.6	49.0	28.9	30.6	45.4
TiO_2	1.9	6.9	7.4	2.4	2.0	1.1
Fe_2O_3	7.1	5.7	6.0	6.3	6.1	6.5
BaO	0.0	4.6	3.5	4.2	2.9	3.3
Total	100	100	100	100	100	100

compositions of selected points are shown in Table 18. The 2-month sample shows significant evidence of sulfation after only 2 months of exposure and was much more pronounced than the 2-month samples for the Baldwin and Columbia Stations that are fired on PRB coals. Figures 38b and 38c show a higher-magnification view of the deposit that is filling the catalyst pores. The deposit consists of particles of fly ash bonded together by a matrix of calcium- and sulfur-rich material, likely in the form of calcium sulfate. The presence of sodium enhances the bonding and sulfation of the particles to form a strongly bonded matrix.

The 4-month sample from the Coyote Station showed particles adhering to the surface and completely filling and masking the pores in the catalyst as shown in Figure 39. Figure 39a shows the external morphology of the catalyst surface showing the masking of the catalyst surface. Chemical compositions of selected points are shown in Table 19. The 4-month sample shows more sulfation than the 2 months of exposure samples. Figures 39b and 39c show a higher-magnification view of the deposit that is filling the catalyst pores. The deposit consists of

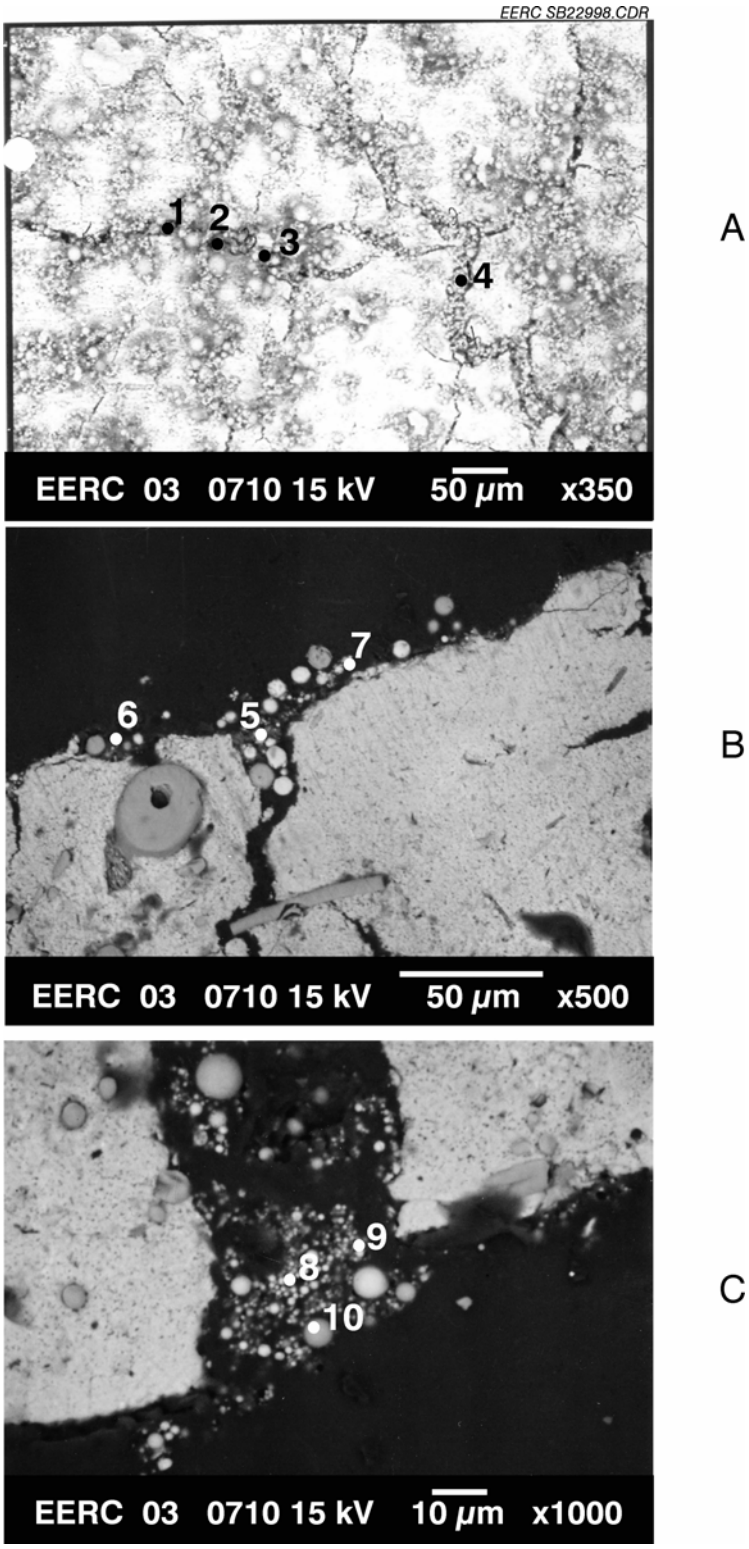

Figure 35. SEM images of ash collected on catalyst surface at the Columbia Station after 2 months of exposure: A) low-magnification image of ash deposit on catalyst surface, B) low-magnification image of polished cross section showing particles in a matrix of calcium- and sulfur-rich materials, and C) higher-magnification image of bonding.

Table 15. Chemical Composition of Selected Points and Areas in Figure 35

	Element, wt%				
	Point 1	Point 2	Point 3	Point 4	Point 5
Oxide					
Na_2O	0.0	0.9	1.3	0.1	0.3
MgO	0.7	1.5	3.2	3.9	0.9
Al_2O_3	12.2	17.6	20.9	12.2	5.9
SiO_2	10.8	4.1	23.3	7.3	6.3
P_2O_5	0.9	0.1	0.0	1.4	2.6
SO_3	15.2	17.6	16.8	17.1	32.3
K_2O	0.2	0.0	0.5	0.0	0.1
CaO	14.1	43.1	25.0	42.0	34.9
TiO_2	44.8	2.8	1.1	10.5	5.2
Fe_2O_3	1.1	12.3	3.9	5.5	11.5
BaO	0.0	0.0	4.2	0.0	0.0
Total	100	100	100	100	100
	Point 6	Point 7	Point 8	Point 9	Point 10
Oxide					
Na_2O	0.0	0.6	1.0	0.5	1.8
MgO	0.0	1.5	2.9	1.4	0.7
Al_2O_3	5.5	12.4	13.6	9.0	20.7
SiO_2	9.4	6.1	15.4	7.9	61.8
P_2O_5	1.2	0.6	1.7	3.1	0.2
SO_3	33.3	22.0	19.5	30.7	0.0
K_2O	0.0	0.0	0.1	0.2	2.5
CaO	44.1	48.5	34.1	38.3	4.4
TiO_2	0.5	4.4	2.4	2.6	2.2
Fe_2O_3	3.1	2.3	6.0	6.3	4.4
BaO	2.8	1.6	3.3	0.0	1.3
Total	100	100	100	100	100

particles of fly ash bonded together by a matrix of sodium-, calcium-, and sulfur-rich material, likely in the form of calcium sulfate. The presence of sodium and potassium enhances the bonding and sulfation of the particles to form a strongly bonded matrix. Significant sodium was found in the deposits, as shown in Table 19.

The 6-month sample from the Coyote Station showed particles adhering to the surface and filling pores in the catalyst, as shown in Figure 40. Figure 40a shows the external morphology of the catalyst surface showing particles trapped in the pores of the catalysts. Chemical compositions of selected points are shown in Table 20. Figures 40b and 40c show a higher-magnification view of the deposit that is filling the catalyst pore. The deposit consists of particles of fly ash bonded together by a matrix of sodium-, calcium- and sulfur-rich material, likely in the form of sulfate. The 6-month samples show the most extensive degree of sulfation of the Coyote Station samples.

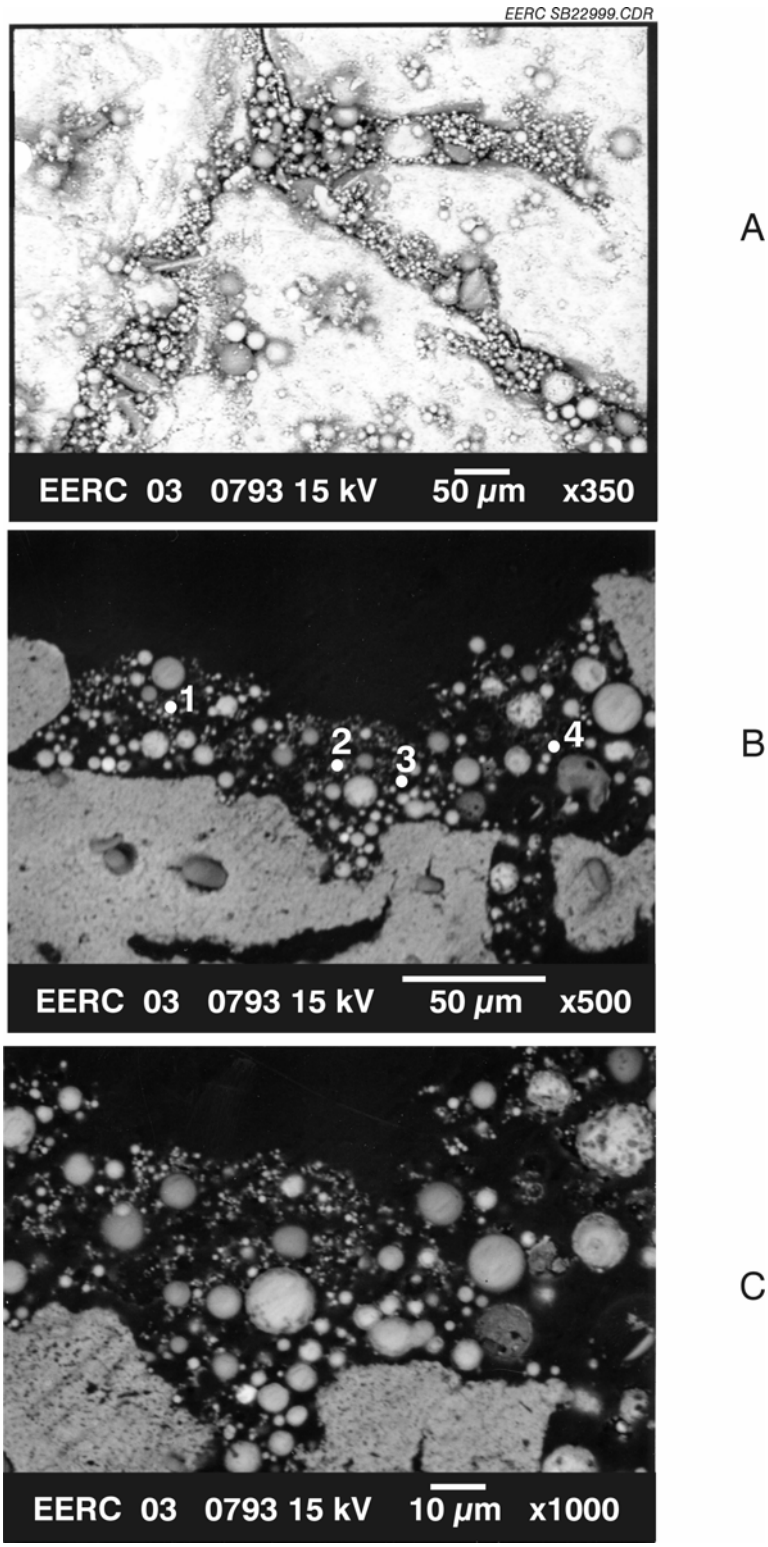

Figure 36. SEM images of ash collected on catalyst surface at the Columbia Station after 4 months of exposure: A) low-magnification image of ash deposit on catalyst surface, B) low-magnification image of polished cross section showing particles in a matrix of calcium- and sulfur-rich materials, and C) higher-magnification image of bonding.

Table 16. Chemical Composition of Selected Points and Areas in Figure 36

	Element, wt%			
	Point 1	Point 2	Point 3	Point 4
Oxide				
Na_2O	0.5	0.0	0.6	0.3
MgO	3.3	1.9	3.2	2.4
Al_2O_3	13.1	10.2	13.0	6.3
SiO_2	12.4	8.4	8.4	3.6
P_2O_5	1.3	0.5	2.1	0.6
SO_3	27.7	29.9	32.2	47.4
K_2O	0.2	0.6	0.1	0.8
CaO	32.1	38.1	28.9	33.2
TiO_2	1.0	2.7	1.3	0.0
Fe_2O_3	6.3	6.3	7.6	2.6
BaO	2.0	1.4	2.5	2.6
Total	100	100	100	100

Reactivity Testing

Samples of the catalyst from 2, 4, and 6 months of operations were submitted to the appropriate catalyst vendor for reactivity testing. The results of only the samples from the Baldwin installation are available at the time of this report. An addendum to this report will be sent when the results from Coyote and Columbia are made available to the EERC.

Table 21 contains the results of the reactivity analysis on the 2-, 4-, and 6-month samples from the Baldwin Station. After 2 months of operation, the catalyst had no noticeable loss of reactivity when compared to the reference catalyst. After 4 months, the reactivity was 96% of the reference, and after 6 months, the reactivity had dropped to 84% of the reference catalyst.

Task 5 – Determination of SCR Blinding Mechanisms

The mechanism for the formation of deposits that blind SCR catalysts involves the transport of very small particles rich in alkali and alkaline-earth elements, the surface of the catalyst, and reactions with SO_2/SO_3 to form sulfates. The formation of SO_3 from SO_2 is catalyzed by the SCR; this, in turn, increases the reaction rate of SO_3 to form sulfates. In some cases, the alkali and alkaline-earth elements will also react with CO_2 to form carbonates. XRD analysis shown in Figure 41 identified $CaSO_4$ as a major phase and $Ca_3Mg(SiO_4)_2$ and $CaCO_3$ as minor phases.

Lignite and subbituminous coals contain high levels of organically associated alkali and alkaline-earth elements, including sodium, magnesium, calcium, and potassium, in addition to mineral phases. The primary minerals present in these coals include quartz, clay minerals, carbonates, sulfates, sulfides, and phosphorus-containing minerals (18).

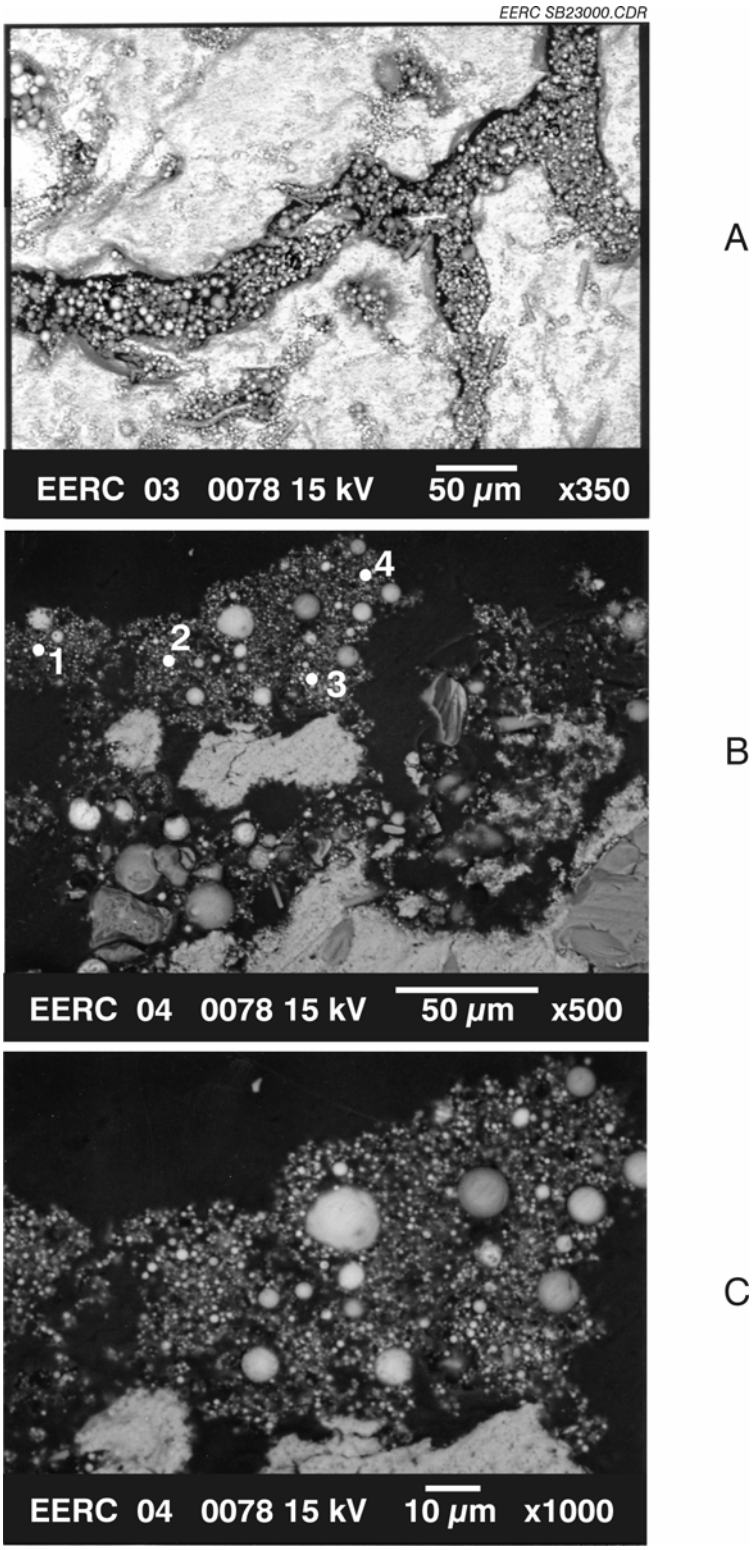

Figure 37. SEM images of ash collected on catalyst surface at the Columbia Station after 6 months of exposure: A) low-magnification image of ash deposit on catalyst surface, B) low-magnification image of polished cross section showing particles in a matrix of calcium- and sulfur-rich materials, and C) higher-magnification image of bonding.

Table 17. Chemical Composition of Selected Points and Areas in Figure 37

	Element, wt%			
	Point 1	Point 2	Point 3	Point 4
Oxide				
Na_2O	0.1	0.0	0.3	0.6
MgO	1.8	0.7	1.7	2.2
Al_2O_3	10.9	9.6	6.2	11.3
SiO_2	13.1	11.3	12.4	19.5
P_2O_5	3.9	4.8	0.2	2.1
SO_3	27.6	34.0	35.5	30.0
K_2O	0.5	0.3	0.1	1.2
CaO	33.0	25.9	39.8	25.8
TiO_2	0.8	2.5	1.6	3.3
Fe_2O_3	6.1	9.7	1.9	2.9
BaO	2.1	1.2	0.0	1.1
Total	100.00	100.00	100.00	100.00

During combustion, the inorganic components in the coal are partitioned into various size fractions based on the type of inorganic component, their association in the coal, and combustion system design and operating conditions. Significant research has been conducted on ash formation mechanisms and relationships and their resulting impacts on power plant performance (18–34). Typically, during combustion the inorganic components associated with western subbituminous and lignite coal are distributed into various size fractions of ash, as shown in Figure 42. The results shown in Figure 42 were obtained from isokinetic sampling, aerodynamically size-fractionating ash particles from a full-scale pc-fired boiler firing subbituminous coal, and analyzing each size fraction. The results show that the smaller-sized fractions of ash are dominated by partially sulfated alkali and alkaline-earth elements. These ash particles are largely derived from the organically associated cations in the coal. The larger-sized fraction has higher levels of aluminum and silicon derived from the mineral fraction of the ash-forming component of the coal.

Entrained ash was extracted from the Columbia Station at the point of the inlet to the SCR reactor and was aerodynamically classified and analyzed. The composition of the size fractions was compared to the chemical composition of the ash deposited on and in the catalyst, as shown in Figure 43. The comparison shows that the composition of the particle captured in the SCR catalyst is very similar to the <5-µm size fraction. The deposited material shows significantly more sulfation than the entrained-ash size fraction, indicating that the sulfation process occurs after the particles are deposited in the catalyst.

The mechanism of SCR catalyst blinding when lignite or subbituminous coals are fired is shown in Figure 44 (35). The requirements for the formation of deposits that blind SCR catalyst include firing a coal that produces significant levels of <5-µm-sized particles. The particles are transported into the pores of the catalyst and subsequently react with SO_3 to form sulfates. The sulfate forms a matrix that bonds other ash particles. The SCR catalyzes the formation of SO_3 and thereby increases the rate of sulfation (9, 15). The sulfation of CaO increases the molar

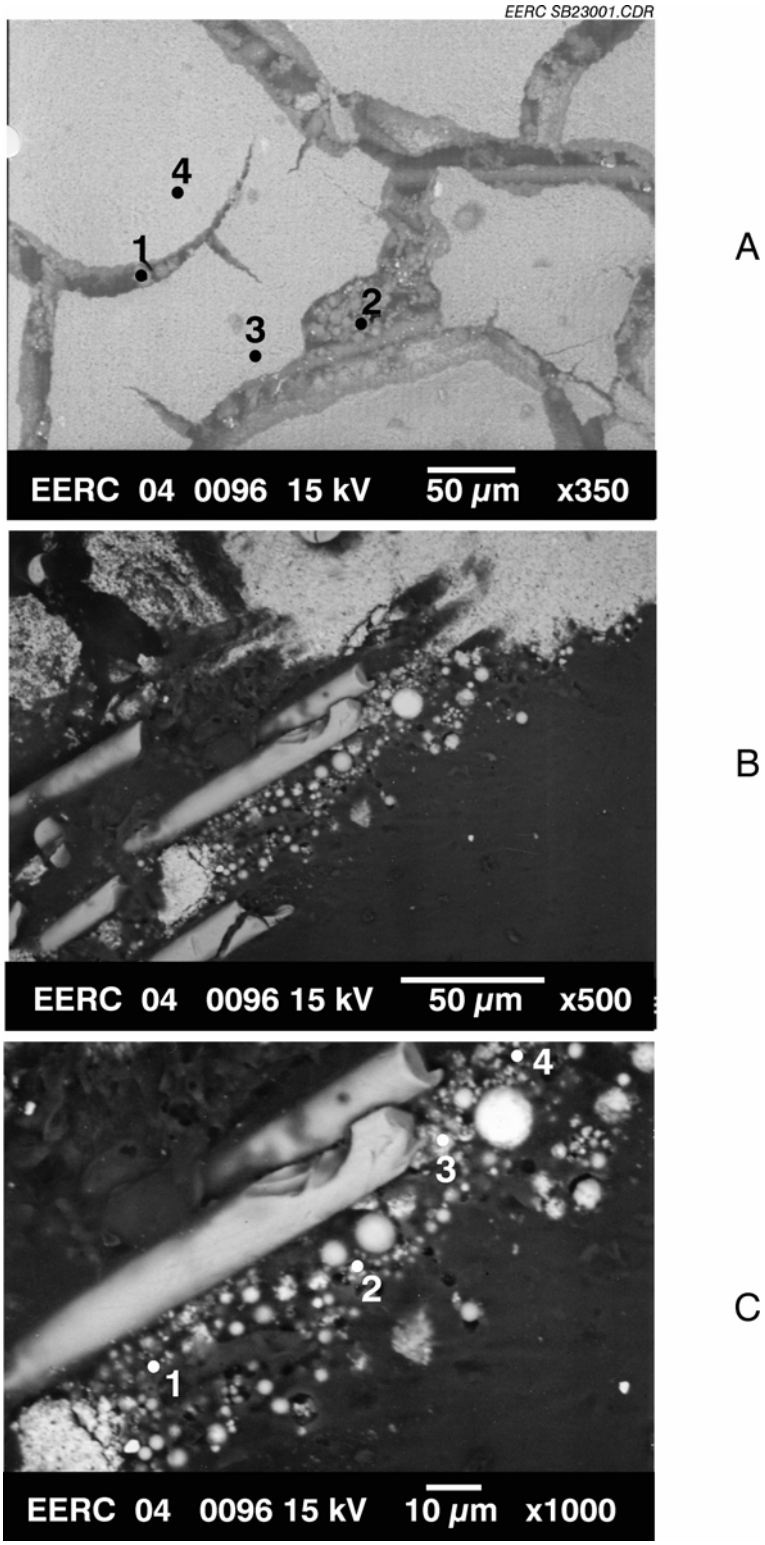

Figure 38. SEM images of ash collected on catalyst surface at the Coyote Station after 2 months of exposure: A) low-magnification image of ash deposit on catalyst surface, B) low-magnification image of polished cross section showing particles in a matrix of calcium- and sulfur-rich materials, and C) higher-magnification image of bonding.

Table 18. Chemical Composition of Selected Points and Areas in Figure 38c

	Point 1	Point 2	Point 3	Point 4
Oxide				
Na_2O	0.9	0.7	1.2	1.0
MgO	5.0	1.6	5.6	1.7
Al_2O_3	12.3	5.8	11.9	5.5
SiO_2	24.6	3.1	21.1	2.6
P_2O_5	0.7	0.0	0.5	0.0
SO_3	23.5	44.0	17.4	31.8
K_2O	0.5	0.3	0.8	0.4
CaO	14.9	36.4	19.6	46.9
TiO_2	7.2	1.9	8.0	2.1
Fe_2O_3	9.2	5.5	11.8	6.9
BaO	1.3	0.7	2.1	1.1
Total	100	100	100	100

volume, resulting in the filling of the pore. For coals that have high sodium contents, formation of low melting point phases such as pyrosulfates are possible (36). Pyrosulfate materials can melt at temperatures as low as 279°C (535°F) in coal-fired power systems.

Add-On Task – Characterization of Mercury Transformations Across SCR Catalysts for a Lignite Coal-Fired Boiler

The ability of mercury to be oxidized across the SCR catalyst was investigated at the Coyote Station. The Coyote Station is fired on North Dakota lignite, and the flue gas is dominated by elemental mercury. Measurement of mercury speciation was conducted using the OH method at the inlet and the outlet of the SCR catalyst. The measurements were made upon installation of the catalyst and after 2 and 4 months of operation. The results of the mercury speciation measurement at the inlet and outlet of the SCR catalyst conducted upon installation are shown in Figure 45. The inlet and outlet measurements were repeated three times and are shown in Figure 45. The level of elemental mercury at the inlet was approximately 76% to 92%, with the remaining in the oxidized form ranging from 8% to 24%. Very little was in the form of particulate mercury at the inlet. Measurement of mercury speciation was conducted with the NH_3 on and off. The results with the NH_3 off showed an increase in the oxidized mercury to 43% of the total mercury occurring across the SCR catalyst. However, when the NH_3 was introduced into the SCR catalyst, the amount of mercury oxidation decreased from 43% to 19%. There was an increase in the particulate mercury from 1.0% to 7.2%.

The mercury oxidation after the SCR catalyst was exposed to flue gas and particulate for 2 months is shown in Figure 46. The level of oxidized mercury at the inlet ranges from 7.5% to 11.1% of the total mercury. The level of oxidized mercury at the outlet ranged from 7.6% to 14% of the total mercury. The level of particulate mercury increased from a negligible level to 3% of the total mercury at the outlet.

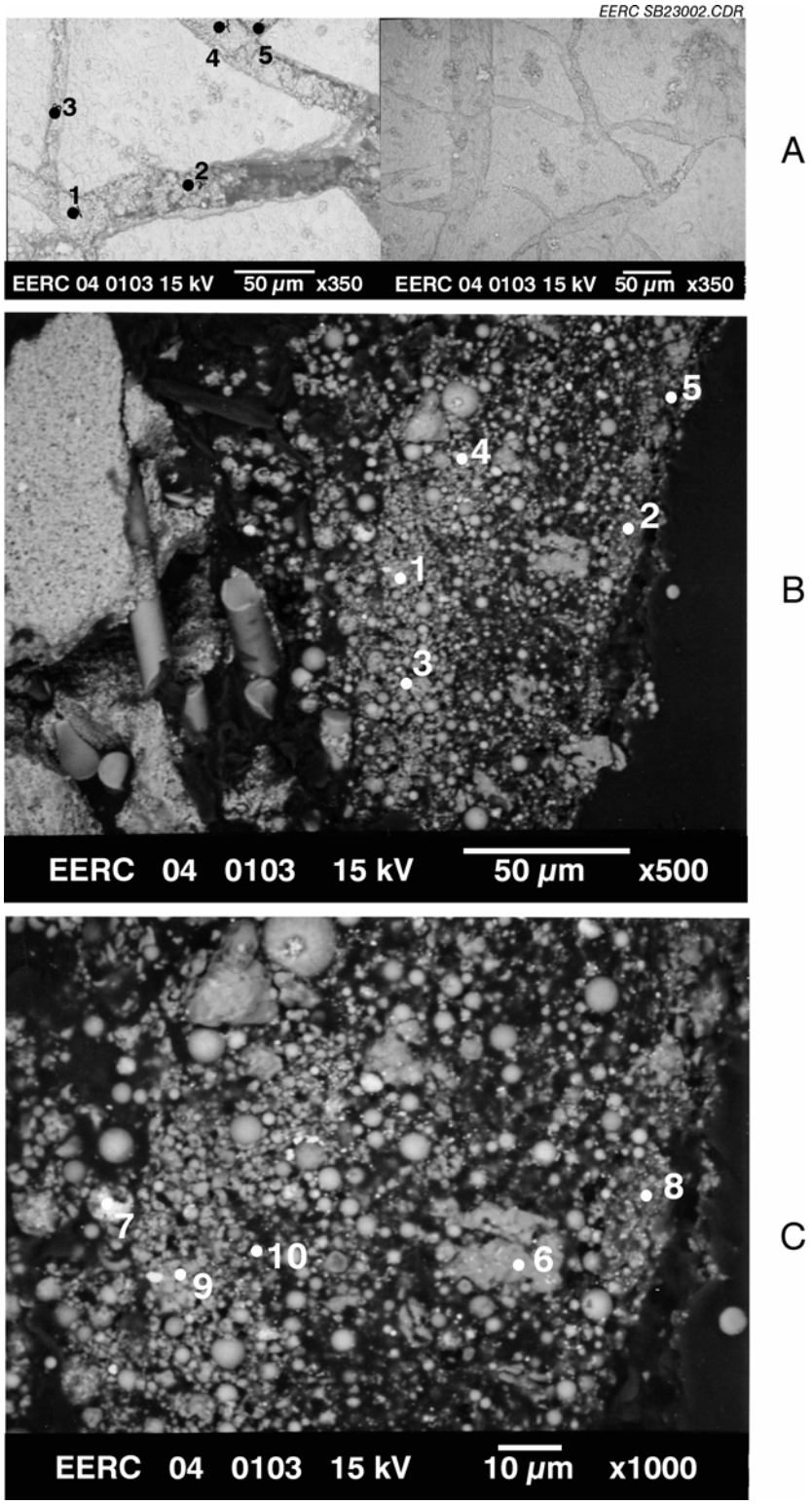

Figure 39. SEM images of ash collected on catalyst surface at the Coyote Station after 4 months of exposure: A) low-magnification image of ash deposit on catalyst surface, B) low-magnification image of polished cross section showing particles in a matrix of calcium- and sulfur-rich materials, and C) higher-magnification image of bonding.

Table 19. Chemical Composition of Selected Points and Areas in Figure 39b and 39c

	Element, wt%				
	Point 1	Point 2	Point 3	Point 4	Point 5
Oxide					
Na_2O	6.7	1.9	7.1	6.2	3.1
MgO	1.1	1.7	1.1	2.6	3.2
Al_2O_3	2.6	8.8	4.0	4.8	10.5
SiO_2	7.0	21.1	11.3	5.6	32.2
P_2O_5	0.2	2.4	0.0	0.2	0.9
SO_3	54.7	38.5	56.4	57.5	30.4
K_2O	2.0	2.8	0.7	2.8	2.4
CaO	18.0	3.4	15.8	9.3	2.3
TiO_2	0.6	0.8	1.1	1.3	1.5
Fe_2O_3	5.8	5.1	2.1	6.5	9.8
BaO	1.4	13.5	0.5	3.4	3.6
Total	100	100	100	100	100
	Point 6	Point 7	Point 8	Point 9	Point 10
Oxide					
Na_2O	9.5	2.6	10.4	8.9	4.4
MgO	1.2	1.9	1.3	3.0	3.7
Al_2O_3	2.6	8.6	4.2	4.9	10.6
SiO_2	6.3	18.2	10.5	5.0	28.9
P_2O_5	0.1	1.9	0.0	0.1	0.7
SO_3	41.8	28.4	44.9	44.5	23.4
K_2O	3.2	4.3	1.2	4.4	3.8
CaO	24.5	4.4	22.5	12.8	3.1
TiO_2	0.6	0.8	1.3	1.5	1.8
Fe_2O_3	7.7	6.6	2.9	8.9	13.2
BaO	2.4	22.3	0.9	5.9	6.3
Total	100	100	100	100	100

The results of mercury oxidation across the SCR catalyst after 4 months of exposure to flue gas and particulate are shown in Figure 47. The results show a higher level of oxidized mercury at the inlet as compared to testing conducted at installation and after 2 months. The level of oxidized mercury at the inlet ranges from 32% to 38% of the total, with about 5% of the total in the particulate form. The outlet levels of oxidized mercury decrease after passing through the catalyst to about 20% of the total. The level of particulate mercury remained about the same across the catalyst.

The results of mercury oxidation across the SCR catalyst after 6 months of exposure to flue gas are shown in Figure 48. The amount of oxidized mercury at the inlet ranges from 6.5% to 10.5% of the total with about 2.0% in the particulate form. The levels of oxidized mercury at the outlet increases slightly to 8.5% to 11.0% of the total mercury, while the particulate bound mercury also increases to as high as 12.0%.

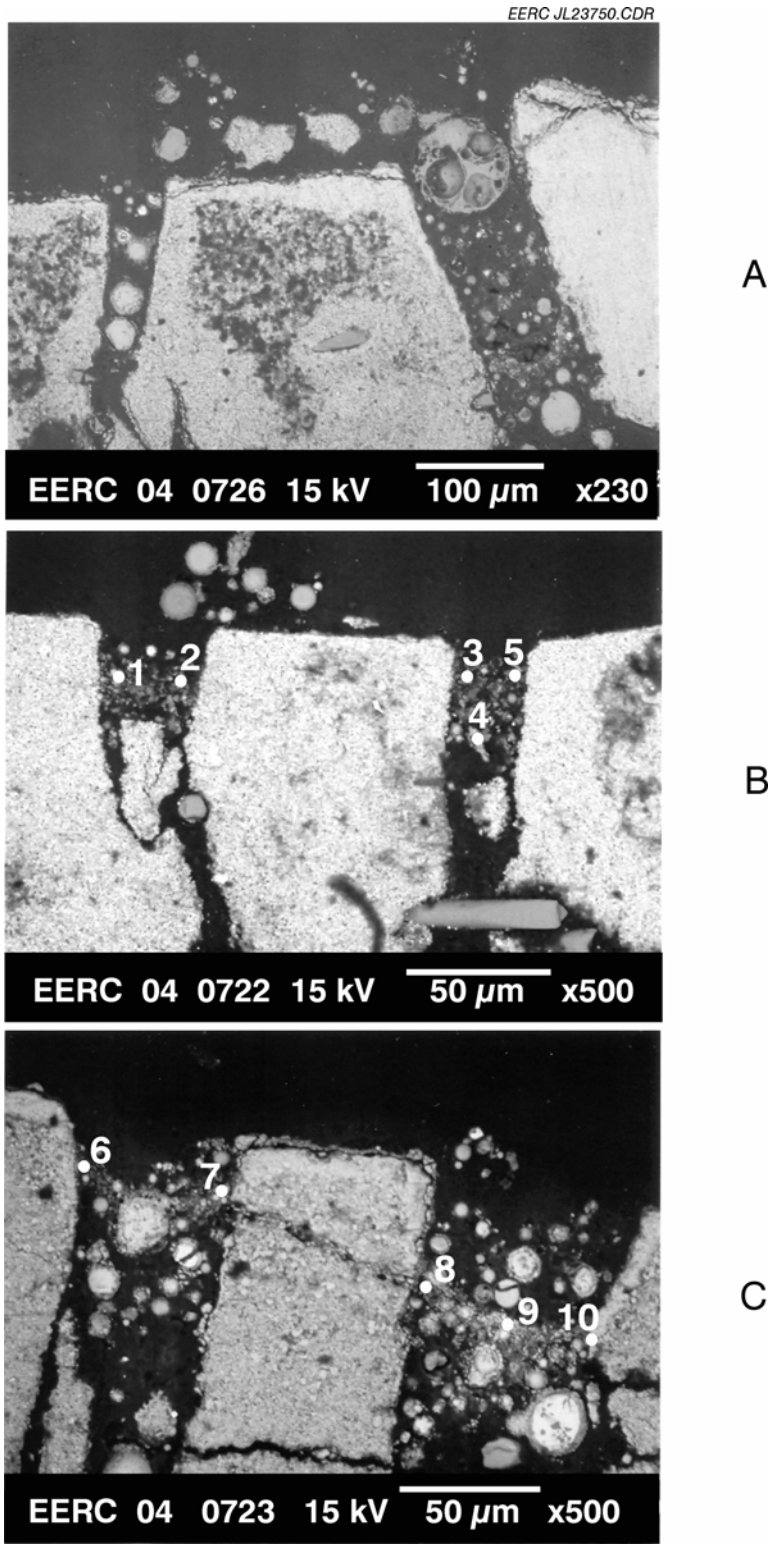

Figure 40. SEM images of ash collected on catalyst surface at the Coyote Station after 6 months of exposure: A) low-magnification image of ash deposit on catalyst surface, B) low-magnification image of polished cross section showing particles in a matrix of calcium- and sulfur-rich materials, and C) higher-magnification image of bonding.

Table 20. Chemical Composition of Selected Points and Areas in Figure 40

	Element, wt%				
	Point 1	Point 2	Point 3	Point 4	Point 5
Oxide					
Na_2O	5.0	3.2	6.6	5.8	4.1
MgO	1.6	0.0	0.0	7.6	1.4
Al_2O_3	2.1	3.3	0.6	0.8	1.7
SiO_2	10.7	12.8	3.6	2.6	14.4
P_2O_5	0.0	0.0	0.0	0.0	0.0
SO_3	57.9	40.7	67.0	71.0	52.7
K_2O	0.5	0.8	0.8	1.3	0.4
CaO	13.7	6.2	12.7	7.7	16.3
TiO_2	2.0	33.0	0.0	1.7	2.1
Fe_2O_3	6.5	0.0	8.8	1.4	7.0
BaO	0.0	0.0	0.0	0.0	0.0
Total	100	100	100	100	100
	Point 6	Point 7	Point 8	Point 9	Point 10
Oxide					
Na_2O	6.5	4.1	5.7	8.1	6.7
MgO	4.6	3.1	4.4	7.5	3.7
Al_2O_3	3.3	10.2	1.6	5.4	2.4
SiO_2	11.5	2.3	4.1	10.1	9.6
P_2O_5	2.2	0.5	0.0	0.9	7.2
SO_3	52.5	48.2	61.4	53.1	56.7
K_2O	1.9	1.0	10.0	3.0	0.9
CaO	13.6	23.9	2.6	8.6	10.5
TiO_2	2.7	3.7	0.7	0.0	0.0
Fe_2O_3	1.2	3.0	9.5	3.3	2.3
BaO	0.0	0.0	0.0	0.0	0.0
Total	100	100	100	100	100

Table 21. Results of Reactivity Tests for the Baldwin Station

Catalyst	K–NO_x 350°C (662°F) (scfh/ft^3)	K/K_o 350°C (662°F)
Reference	22,808	—
2 month	23,400	1.03
4 month	21,361	0.96
6 month	19,510	0.84

Task 6 – Final Interpretation, Recommendations, and Reporting

Lignite and subbituminous coals contain high levels of organically bound alkali and alkaline-earth elements, including sodium, calcium, potassium, and magnesium. During combustion, partitioning of these elements occurs based on the size of particles, their association in the coal, and system configuration. This phenomenon, coupled with the fact that SCR catalyst

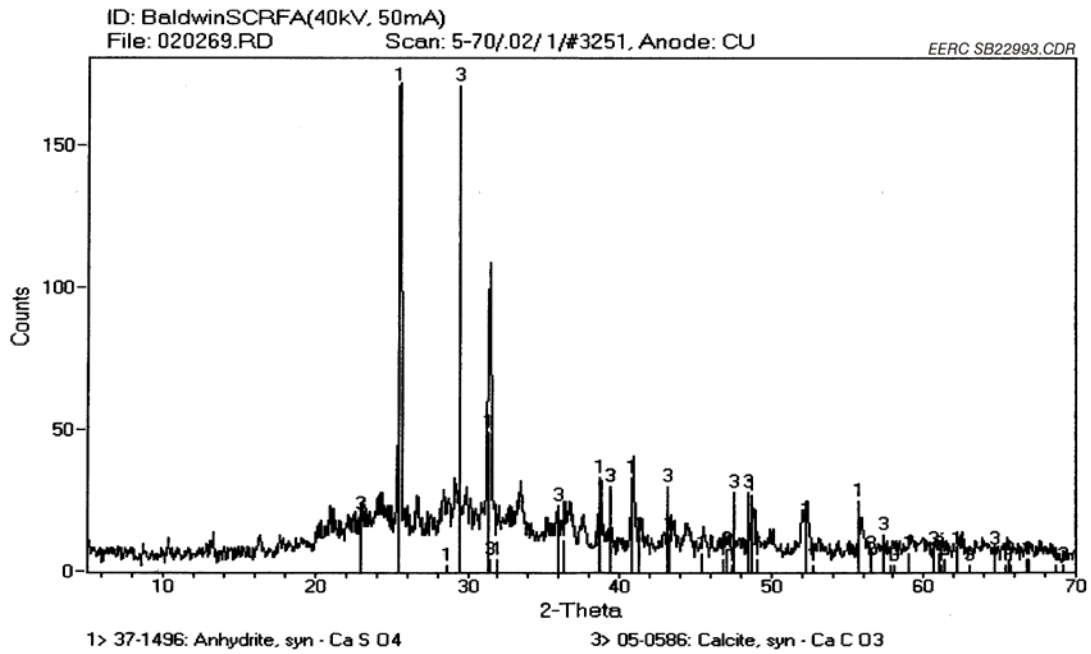

Figure 41. X-ray diffraction of ash collected on SCR catalyst (1 – $CaSO_4$, 2 – $Ca_3Mg(SiO_4)_2$, and 3 – $CaCO_3$).

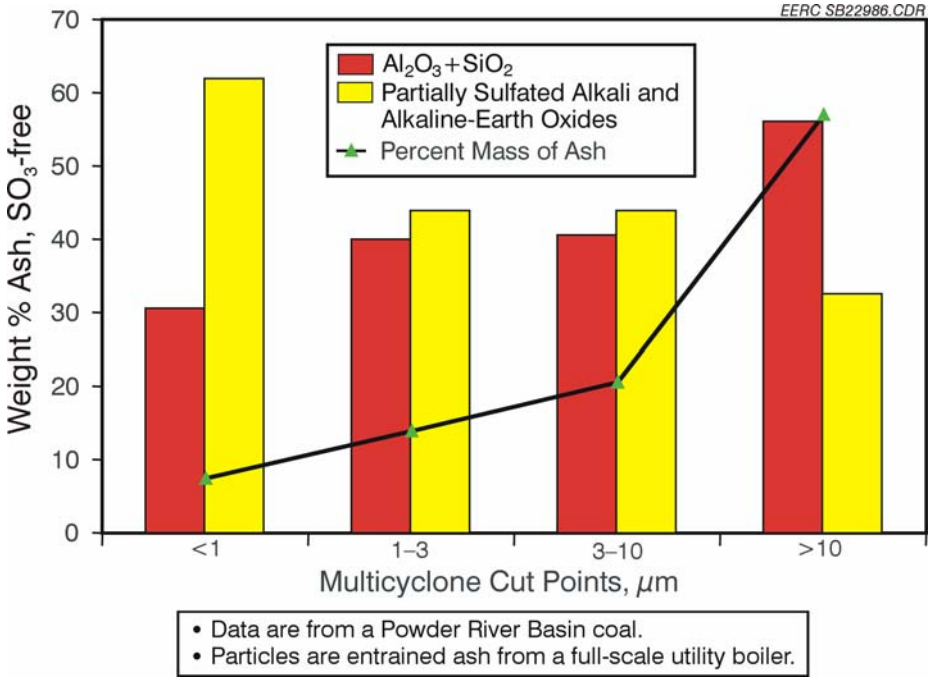

Figure 42. Simplified illustration of ash partitioning in combustion systems (18).

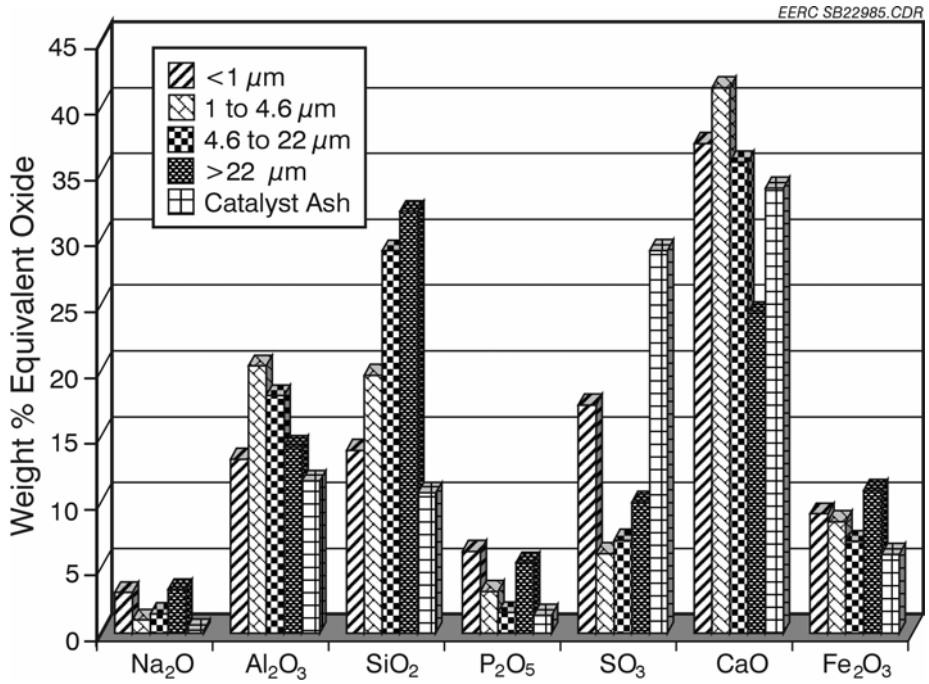

Figure 43. Comparison of entrained ash and deposited ash on catalyst for Columbia Station.

increases the oxidation of SO_2 to SO_3, will lead to extensive blinding of SCR catalyst by the formation of alkali or alkaline-earth sulfates. The results of this study lead the authors to suggest careful evaluation of each SCR installation on applications using subbituminous coals and suggest no installations of SCRs on plants firing lignite coal until further evaluations or improvements to the current technology can be carried out. Installations involving lignite fuels will need advanced cleaning techniques to handle the high-sodium and high-dust loads associated with burning most lignite fuels. The presence of SCR catalyst did not enhance mercury oxidation in the lignite-fired combustion system tested in this study.

CONCLUSIONS

The EERC evaluated the effects that ash from lignite- and PRB-fired combustion has on the performance of SCR catalyst. In order to conduct these tests, a slipstream reactor was designed to expose the SCR catalyst to coal combustion-derived flue gases and particulates. The system is computer-controlled and operates in an automated mode. The system can be operated and monitored remotely through a modem connection. SCR catalyst testing was conducted at two subbituminous-fired plants and one lignite-fired plant. The boiler configurations for the subbituminous-fired plants included a cyclone- and a tangentially fired boiler. The lignite plant was cyclone-fired.

The pressure drop across the catalyst was found to be the most significant for the lignite-fired plant as compared to the subbituminous-fired plants. Both coals had significant accumulations of ash on the catalyst, on both macroscopic and microscopic levels. On a

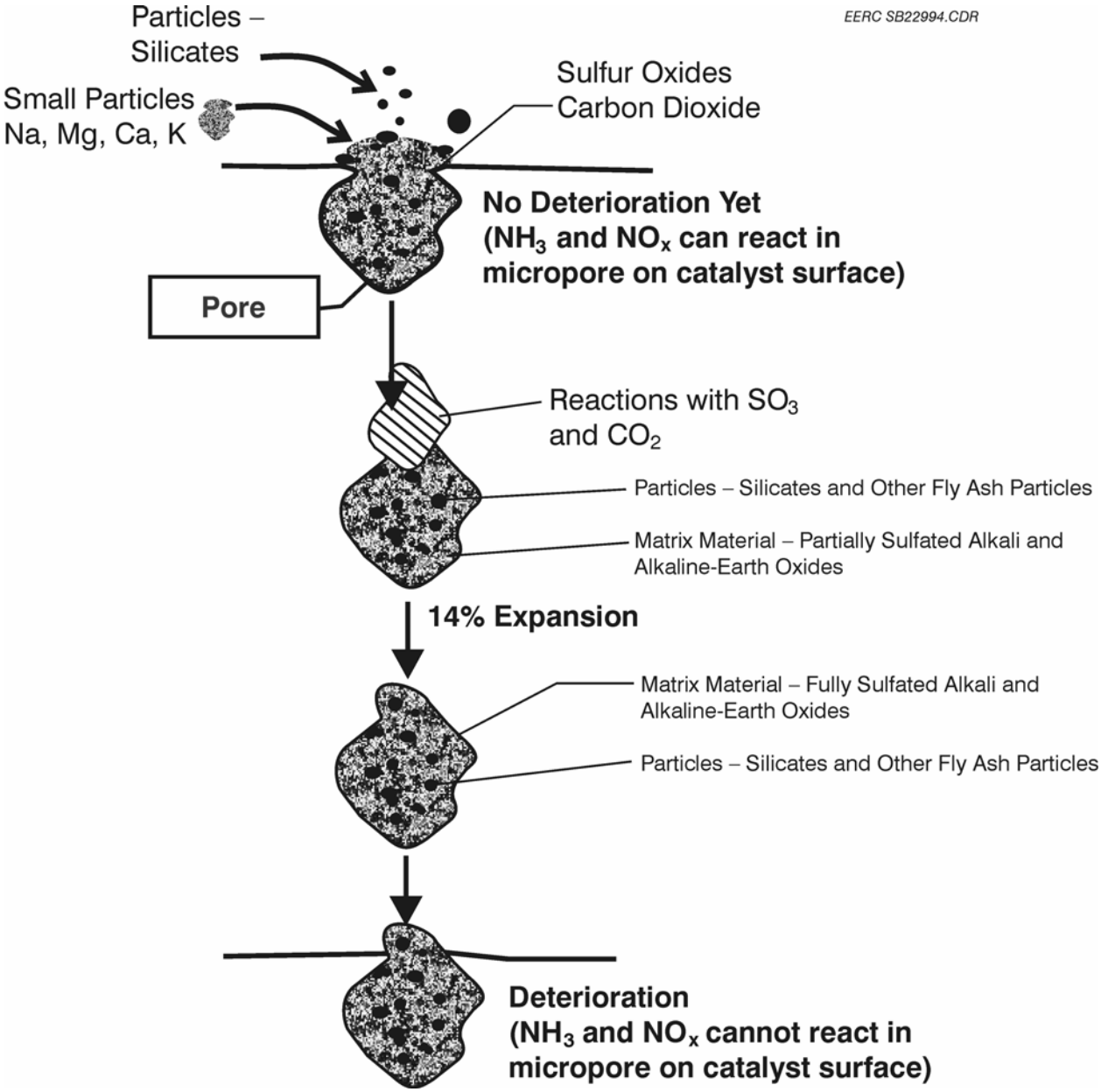

Figure 44. Mechanism of SCR catalyst blinding via the formation of sulfates and carbonates (modified after Pritchard and others [35]).

macroscopic level, there were significant observable accumulations that plugged the entrance as well as the exit of the catalyst sections. On a microscopic level, the ash materials filled pores in the catalyst and, in many cases, completely masked the pores within 4 months of operation. After 6 months of operation, the reactivity of the catalyst from the Baldwin Station was 84% of a comparable reference value.

The deposits on the surfaces and within the pores of the catalyst consisted mainly of sulfated alkali and alkaline-earth element-rich phases. The mechanism for the formation of the

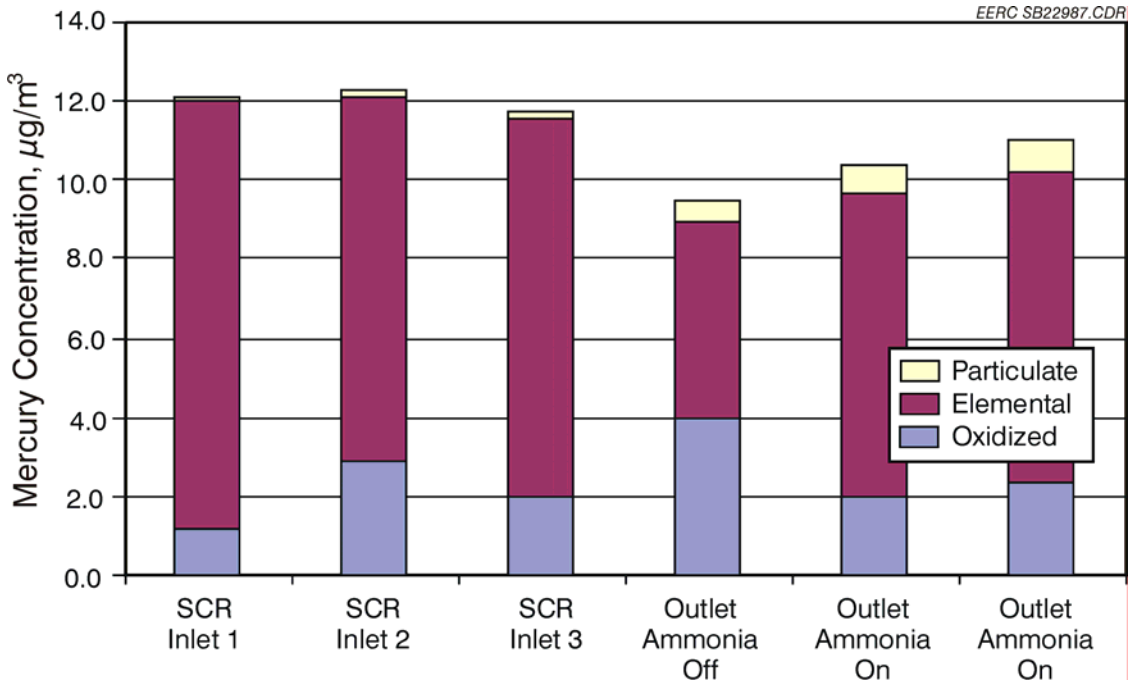

Figure 45. Mercury speciation measurement at the inlet and outlet of the SCR catalyst upon installation of the catalyst.

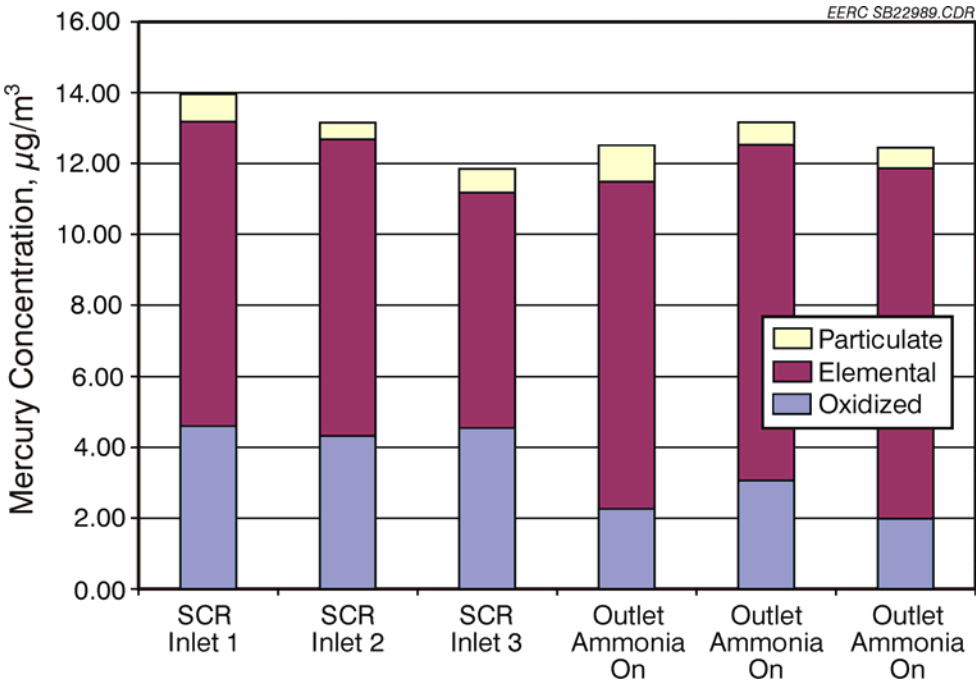

Figure 46. Mercury speciation measurement at the inlet and outlet of the SCR catalyst after exposure to flue gas and particulate for 4 months.

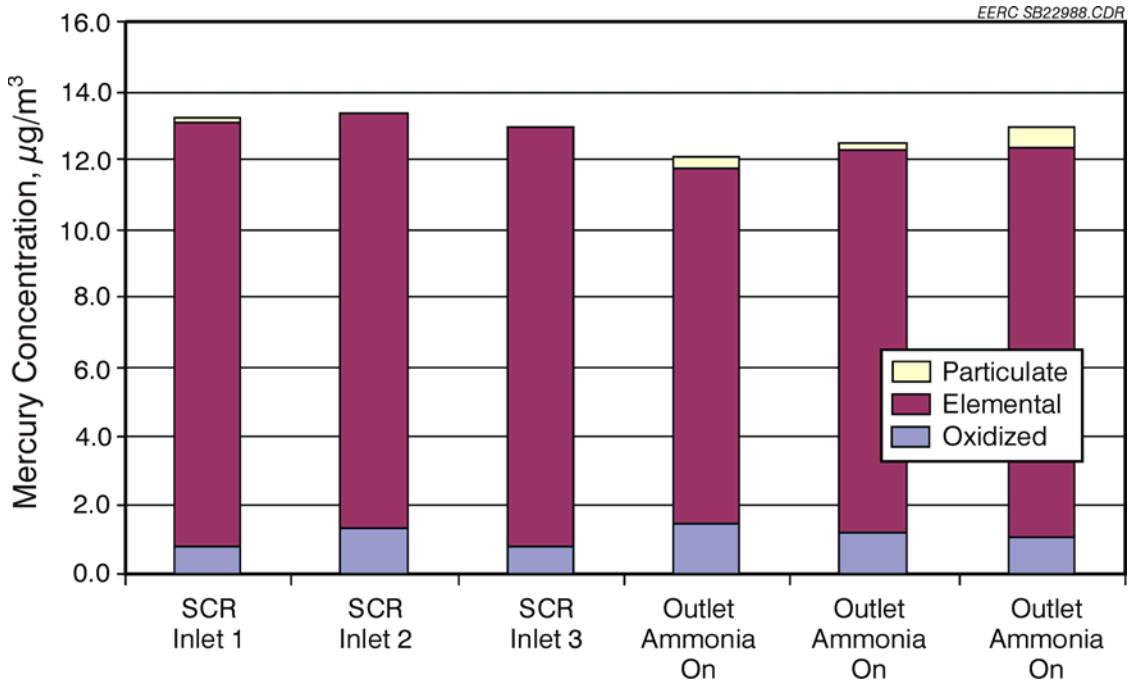

Figure 47. Mercury speciation measurement at the inlet and outlet of the SCR catalyst after exposure to flue gas and particulate for 2 months.

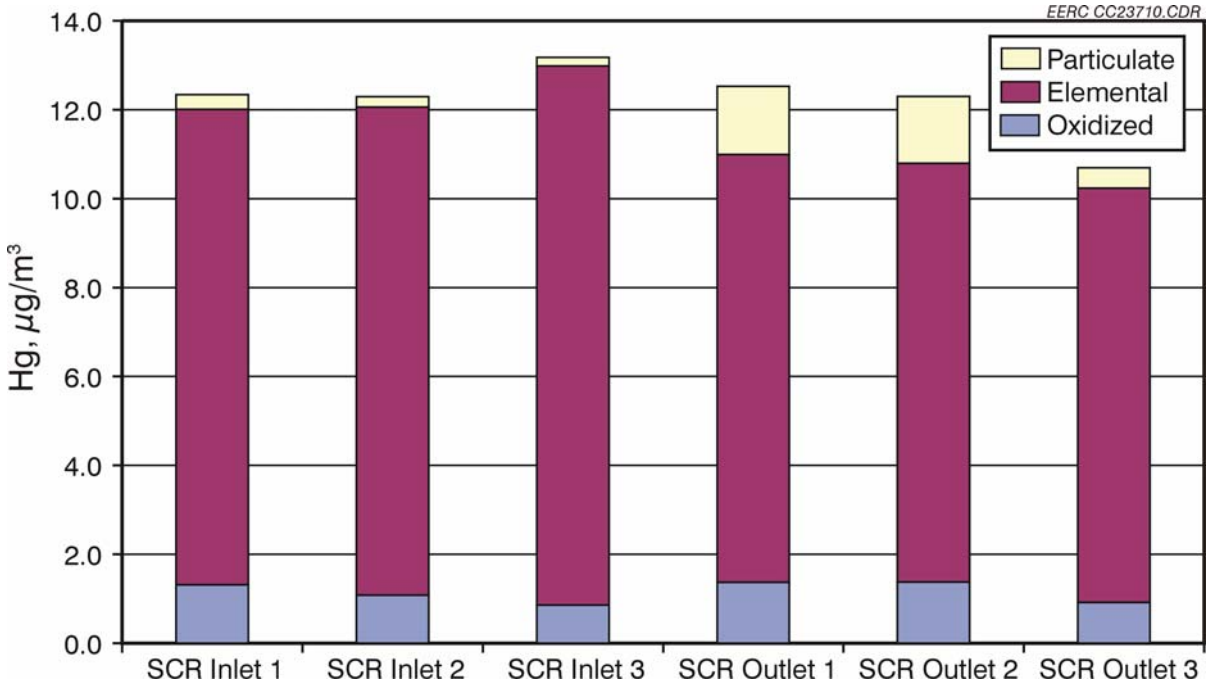

Figure 48. Mercury speciation measurement at the inlet and outlet of the SCR catalyst after exposure to flue gas and particulate for 6 months.

sulfate materials involves the formation of very small particles rich in alkali and alkaline-earth elements, transport of the particles to the surface of the catalyst, and reactions with SO_2–SO_3 to form sulfates. XRD analysis identified $CaSO_4$ as a major phase and $Ca_3Mg(SiO_4)_2$ and $CaCO_3$ as minor phases. These results are consistent with the bench-scale TGA and FACT modeling results. The only exception may be the absence of phosphate materials predicted in the FACT modeling; one possible explanation is that FACT considers each reaction independently and does not consider the selectivity of one reaction over another.

Lignite and subbituminous coals contain high levels of organically associated alkali and alkaline-earth elements, including sodium, magnesium, calcium, and potassium in addition to mineral phases. During combustion, the inorganic components in the coal are partitioned into various size fractions based on the type of inorganic component and their association in the coal and combustion system design and operating conditions. The results of this testing found that the smaller-sized fractions of ash are dominated by partially sulfated alkali and alkaline-earth elements. The composition of the size fractions was compared to the chemical composition of the ash deposited on and in the catalyst. The comparison shows that the composition of the particle captured in the SCR catalyst is very similar to the <5-µm size fraction.

This study suggests careful evaluation of each SCR installation in applications using subbituminous and lignite coals. Improvements are needed to ensure technical feasibility, especially with lignite-fired units. Installations involving lignite fuels will need advanced cleaning techniques to handle the high sodium and high dust loads associated with burning most lignite fuels.

The ability of mercury to be oxidized across the SCR catalyst was investigated at the Coyote Station. The Coyote Station is fired on North Dakota lignite, and the flue gas is dominated by elemental mercury. Measurement of mercury speciation was conducted using the OH method at the inlet and the outlet of the SCR catalyst. These results show limited oxidation of mercury across the SCR catalyst when lignite coals are fired. The reasons for the lack of mercury oxidation include the following: no chlorine present in the coal and flue gas to catalytically enhance the oxidation of Hg^0, higher levels of alkali and alkaline-earth elements acting as sorbents for any chlorine present in the flue gas, and lower levels of acid gases present in the flue gas.

REFERENCES

1. Benson, S.A.; Fegley, M.M., Hurley, J.P.; Jones, M.L.; Kalmanovitch, D.P.; Miller, B.G.; Miller, S.F.; Steadman, E.N.; Schobert, H.H.; Weber, B.J.; Weinmann, J.R.; Zobeck, B.J. *Project Sodium: A Detailed Evaluation of Sodium Effects in Low-Rank Coal Combustion Systems*; Final Technical Report; EERC publication, July 1988.
2. Hurley, J.P.; Erickson, T.A.; Benson, S.A.; Brobjorg, J.N.; Steadman, E.N.; Mehta, A.K.; Schmidt, C.E. *Ash Deposition at Low Temperatures in Boilers Firing Western U.S. Coals*; International Joint Power Generation Conference, Elsevier Science, 1991; pp 1–8.

3. Licata, A.; Hartenstein, H.U.; Gutberlet, H. Utility Experience with SCR in Germany. Presented at the 16th Annual International Pittsburgh Coal Conference, Pittsburgh, PA, Oct 11–15, 1999.
4. Galbreath, K.C.; Zygarlicke, C.J.; Olson, E.S.; Pavlish, J.H.; Toman, D.L. Evaluating Mercury Transformations in a Laboratory-Scale Combustion System. *Science of the Total Environment* **2000**, *261* (1–3).
5. Gutberlet, H.; Spiesberger, A.; Kastner, F.; Tembrink, J. Mercury in Bituminous Coal Furnaces with Flue Gas Cleaning Plants. *VGB Kraftwerkstechnik* **1992**, *72*, 586–691.
6. Laudal, D.L. *Fundamental Study of the Impact of SCR on Mercury Speciation*; Final Report, Center for Air Toxic Metals, 03-EERC-12-03, Dec 2003.
7. Gutberlet, H.; Schlüten, A.; Licata, A. SCR Impacts on Mercury Emissions on Coal-Fired Boilers. Presented at EPRI Workshop, Memphis, TN, April 2002.
8. Laudal, D.L. *Effect of Selective Catalytic Reduction on Mercury – 2002 Field Study Update*; EPRI, Palo Alto, CA; the U.S. Department of Energy National Energy Technology Laboratory, Pittsburgh, PA; and the U.S. Environmental Protection Agency, National Risk Management Research Laboratory, Air Pollution and Control Division, Research Triangle Park, NC, 2002.
9. Crocker, C.R.; Benson, S.A.; Laumb, J.D. SCR Catalyst Blinding Due to Sodium and Calcium Sulfate Formation. *Prepr. Pap.—Am. Chem. Soc., Div. Fuel Chem.* **2004**, *49* (1), 169.
10. Benson, S.A.; Laumb, J.D.; Crocker, C.R. Blinding of the SCR Catalysts in Lignite and Subbituminous Coal-Fired Power Plants. Presented at the Clearwater Conference on Coal Utilization and Fuel Systems, Clearwater, FL, April 18–22, 2004.
11. Senior, C.L.; Linjewile, T.; Denison, M.; Swensen, D.; Shino, D.; Bockelie, M.; Baxter, L.; Bartholonew, C.; Hecker, W.; Guo, X.; Nackos, A.; Whitty, K.; Eddings, E. SCR Deactivation Mechanisms Related to Alkali and Alkaline Earth Elements. Presented at the 2003 Conference on Selective Catalytic Reduction (SCR) and Selective Non-Catalytic Reduction (SNCR) for NO_x Control, Pittsburgh, PA, Oct 29–30, 2003.
12. Rigby, K.; Johnson, R.; Neufort, R.; Gunther, P.; Hurns, E.; Klatt, A.; Sigling, R. SCR Catalyst Design Issues and Operating Experience: Coals with High Arsenic Concentrations and Coals from the Powder River Basin. Presented at the International Joint Power Generation Conference, IJPGC2000-15067, July 23–26, 2000.
13. Licata, A.; Hartenstein, H.U.; Gutberlet, H. Utility Experience with SCR in Germany. 16th Annual International Pittsburgh Coal Conference, Pittsburgh, PA. Oct 11–15, 1999.
14. Cichanovicz, J.E.; Muzio, J. Twenty-Five Years of SCR Evolution: Implications for U.S. Applications and Operation. EPRI–DOE–EPA Combined Utility Air Pollution Control Symposium: The MEGA Symposium, AWMA, Chicago, IL, Aug 20–23, 2001.
15. Laumb, J.D.; Benson, S.A. Bench- and Pilot-Scale Studies of SCR Catalyst Blinding. In *Proceedings of Power Production in the 21st Century: Impacts of Fuel Quality and Operations*; United Engineering Foundation, Snowbird, UT, Oct 2001.
16. Wieck-Hansen, K. Cofiring Coal and Straw in PF Boilers: Performance Impact of Straw with Emphasis on SCR Catalyst for $DeNO_x$ Catalysts. Presented at the 16th Annual International Pittsburgh Coal Conference, Oct 11–15, 1999.
17. Khodayari, R.; Odenbrand, C.U.I. Regeneration of Commercial TiO_2–V_2O_5–WO_3 SCR Catalysts Used in Bio Fuel Plants. *Applied Catalysis B: Environmental* **2001**, *30*, 87–99. Elsevier.

18. Benson, S.A.; Jones, M.L.; Harb, J.N. Ash Formation and Deposition: Chapter 4, In *Fundamentals of Coal Combustion for Clean and Efficient Use*; Smoot, L.D., Ed.; Elsevier: Amsterdam, 1993, 299–373.
19. ASTM Method D6784-02. Standard Test Method for Elemental, Oxidized, Particle-Bound and Total Mercury in Flue Gas Generated from Coal-Fired Stationary Sources (Ontario Hydro Method). http://www.astm.org/cgi-bin/SoftCart.exe/DATABASE.CART/PAGES/D6784.htm?E+mystore (accessed August 2004).
20. Schobert, H.H. *Lignites of North America*; Coal Science and Technology 13, Elsevier: New York, 1995.
21. Baxter, L.; DeSollar, R., Eds. *Applications of Advanced Technology to Ash-Related Problems in Boilers*; Plenum Press: New York, 1996.
22. Couch, G. *Understanding Slagging and Fouling During pf Combustion*; IEA Coal Research Report, 1994.
23. Williamson, J.; Wigley, F., Eds. The Impact of Ash Deposition on Coal Fired Plants. In *Proceedings of the Engineering Foundation Conference*; Taylor & Francis, London, 1994.
24. Benson, S.A., Ed. *Inorganic Transformations and Ash Deposition During Combustion*; American Society of Mechanical Engineers for the Engineering Foundation, New York, 1992.
25. Bryers, R.W.; Vorres, K.S., Eds. *Proceedings of the Engineering Foundation Conference on Mineral Matter and Ash Deposition from Coal*; Santa Barbara, CA, Feb 22–26, 1988, United Engineering Trustees Inc., 1990.
26. Raask, E. *Erosion Wear in Coal Utility Boilers*; Hemisphere: Washington, 1988.
27. Raask, E. *Mineral Impurities in Coal Combustion*; Hemisphere: Washington, 1985.
28. Benson, S.A., Ed. *Ash Chemistry: Phase Relationships in Ashes and Slags*; Special Issue of Fuel Processing Technology, Elsevier Science Publishers, Amsterdam, 1998; Vol. 56, Nos. 1–2, 168 p.
29. Laumb, M.; Benson, S.A.; Laumb, J. Ash Behavior in Utility Boilers: A Decade of Fuel and Deposit Analyses. Presented at the United Engineering Foundation Conference on Ash Deposition and Power Production in the 21st Century, Snowbird, UT, Oct 28 – Nov 2, 2001.
30. Benson, S.A.; Hurley, J.P.; Zygarlicke, C.J.; Steadman, E.N.; Erickson, T.A. Predicting Ash Behavior in Utility Boilers. *Energy Fuels* **1993**, *7* (6), 746–754.
31. Sarofim, A.F.; Howard, J.B.; Padia, A.S. The Physical Transformations of Mineral Matter in Pulverized Coal under Simulated Combustion Conditions. *Combust. Sci. Technol.* **1977**, *16*, 187.
32. Loehden, D.; Walsh, P.M.; Sayre, A.N.; Beer, J.M.; Sarofim, A.F. Generation and Deposition of Fly Ash in the Combustion of Pulverized Coal. *J. Inst. Energy* **1989**, 119–127.
33. Zygarlicke, C.J.; Toman, D.J.; Benson, S.A. Trends in the Evolution of Fly Ash Size During Combustion. *Prepr. Pap.—Am. Chem. Soc., Div. Fuel Chem.* **1990**, *35* (3), 621–636.
34. Mehta, A.; Benson, S.A., Eds. *Effects of Coal Quality on Power Plant Management: Ash Problems, Management, and Solutions*; United Engineering Foundation Inc., New York, and EPRI, Palo Alto, CA, 2001.

35. Pritchard, S.; Hellard, D.; Cochran, J. Catalyst Design Experience for 640-MW Cyclone Boiler Fired with 100% PRB Fuel. http://www.cormetech.com/techdata/index.html (accessed August 2004).
36. Singer, J.P. *Combustion, Fossil Power Systems*; Combustion Engineering Inc.: Windsor, CT, 1981.